SUPPORTING INFORMATION for

Controlling Product Selectivity During Dioxygen Reduction with Mn Complexes Using Pendent Proton Donor Relays and Added Base

Emma N. Cook, Ian M. Courter, Diane A. Dickie, and Charles W. Machan*

* - machan@virginia.edu; ORCID 0000-0002-5182-1138

E.N.C. ORCID 0000-0002-0568-3600; D.A.D. ORCID 0000-0003-0939-3309

Department of Chemistry, University of Virginia, PO Box 400319, Charlottesville, VA 22904-4319

Table of Contents

Materials and Methods

General Considerations

All chemicals and solvents (ACS or HPLC grade) were commercially available and used as received unless otherwise indicated. For all air-sensitive reactions and electrochemical experiments, HPLC-grade solvents were obtained as anhydrous and air-free from a PPT Glass Contour Solvent Purification System. Gas cylinders were obtained from Praxair (Ar as 5.0; O2 as 4.0) and passed through activated molecular sieves prior to use. Gas mixing for variable concentration experiments was accomplished using a gas proportioning rotameter from Omega Engineering. UV-vis absorbance spectra were obtained on a Cary 60 from Agilent. An Anton-Parr Multiwave Pro SOLV, NXF-8 microwave reactor was used for microwave syntheses. The concentration of O2 saturation in MeCN is reported to be 8.1 mM and the saturation concentration in MeCN with added electrolyte to be 6.3 mM.[1]

Synthesis and Characterization

Synthesis of Mn($^{p\text{-}tbu}$dhbpy)Cl

$^{p\text{-}tbu}$dhbpy[H]$_2$ was synthesized according to our previously reported procedure.[2] Mn($^{p\text{-}tbu}$dhbpy)Cl was synthesized according to previously reported procedures.[3] To a 2-neck, 100 mL round bottom flask, $^{p\text{-}tbu}$dhbpy[H]$_2$ (0.200 g, 0.442 mmol) was added with 50 mL of methanol and allowed to reflux for 1 h. Then, manganese(II) acetate tetrahydrate (0.108 g, 0.442 mmol) was added with dichloromethane (10 mL) and sparged with compressed air for 2 minutes. The dark green solution was allowed to reflux for 3 hours. After this time, saturated NaCl solution (50 mL) was added to the flask resulting in a dark reddish-brown suspension. The suspension was filtered, dissolved in DCM, and extracted with saturated NaCl solution (3 x 100 mL). The organic layer was separated, dried over $MgSO_4$ and the solvent was removed under reduced pressure to yield a reddish-brown solid. The solid was then dissolved in 1:1 DCM:MeCN, passed through a syringe filter and the solvent was removed under pressure to yield a reddish-brown solid. Finally, the solid was recrystallized in DCM and hexanes to yield a spectroscopically pure product in 46% yield (0.203 mmol, 0.11 g). Elemental analysis for $C_{30}H_{30}ClMnN_2O_2$ calc'd: C 66.61; H 5.59; N 5.18, found: C 66.31, H 5.98, N 5.15. ESI-MS (*m/z*) $[M - Cl]^+$: calc'd: 505.1688; found 505.1675.

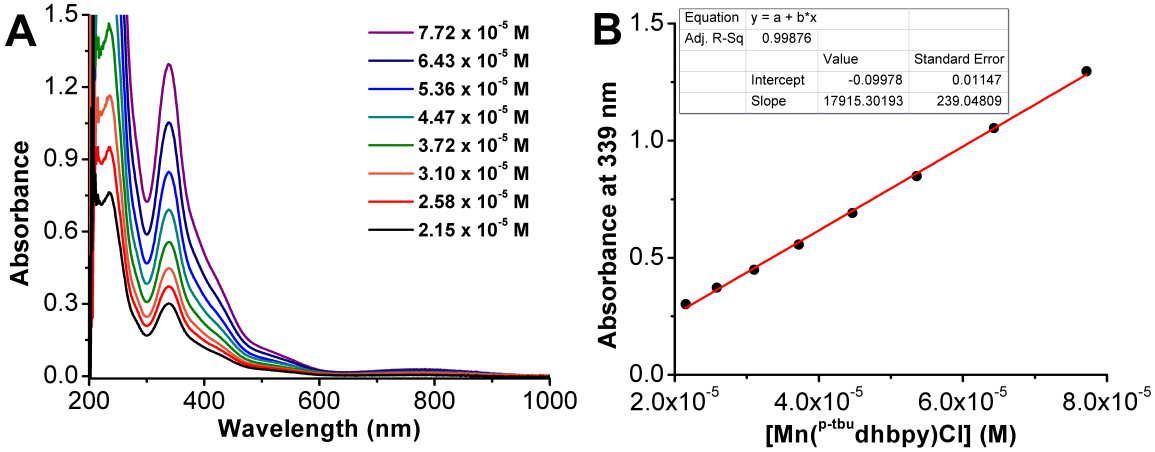

Figure S1. (A) UV-vis serial dilution absorbance data from Mn($^{p\text{-}tbu}$dhbpy)Cl **1** in MeCN solution. Conditions: varying concentration; quartz cell with 1 cm pathlength. (B) Plot of absorbance concentration (M) for Mn($^{p\text{-}tbu}$dhbpy)Cl 1 in MeCN solution at 339 nm (17915 M^{-1} cm^{-1}); R^2=0.999. All: λ_{max} = 236 nm (44786 $M^{-1}cm^{-1}$), 422 nm (5320 $M^{-1}cm^{-1}$), 525 nm (1269 $M^{-1}cm^{-1}$), 777 nm (410 $M^{-1}cm^{-1}$).

Table S1. Summary of Evans' Method Data from Mn($^{p\text{-}tbu}$dhbpy)Cl **1** in *N,N′*-DMF (chosen for solubility reasons) supporting a high-spin d^4 complex.

Trial	Chemical Shift (ppm)	Chemical Shift (Hz)	Total Magnetic Moment (emu mol^{-1})	Paramagnetic Moment (emu mol^{-1})	μ_{eff} (Bohr Magnetons)
1	0.12	72	8.94 x 10^{-3}	9.33 x 10^{-3}	4.72
2	0.12	72	8.94 x 10^{-3}	9.33 x 10^{-3}	4.72
3	0.13	78	9.69 x 10^{-3}	1.01 x 10^{-2}	4.90

Synthesis of Mn(^{nPr}dhbpy)Cl

^{nPr}dhbpy[H]$_2$ was synthesized according to our previously reported procedure. Mn(^{nPr}dhbpy)Cl was synthesized according to previously reported procedures. To a 2-neck, 100 mL round bottom flask, ^{nPr}dbhpy[H]$_2$ (0.195 g, 0.4 mmol) was brought to reflux in 75 mL methanol for 1 h. After this time, manganese(II) acetate tetrahydrate (0.104 g, 0.4 mmol) and DCM (10 mL) were added to the reaction mixture and the solution was sparged with compressed air for 2 minutes, which then turned dark green. After refluxing for 5 hours, saturated NaCl was added (75 mL). The suspension was filtered, dissolved in DCM, and extracted with saturated NaCl (3 x 100 mL). The organic layer was separated and dried over $MgSO_4$, passed through a syringe filter and the solvent was reduced under pressure to yield a dark brown solid. The solid was recrystallized in minimal THF and excess hexanes to yield pure product in 24% yield (55 mg). Elemental analysis for $C_{30}H_{30}ClMnN_2O_2$•1/3CH_2Cl_2 calc'd: C 60.59; H 5.14; N 4.66, found: C 60.45, H 5.02, N 5.07. ESI-MS (*m/z*) [M – Cl]$^+$: calc'd: 537.1586; found 537.1564.

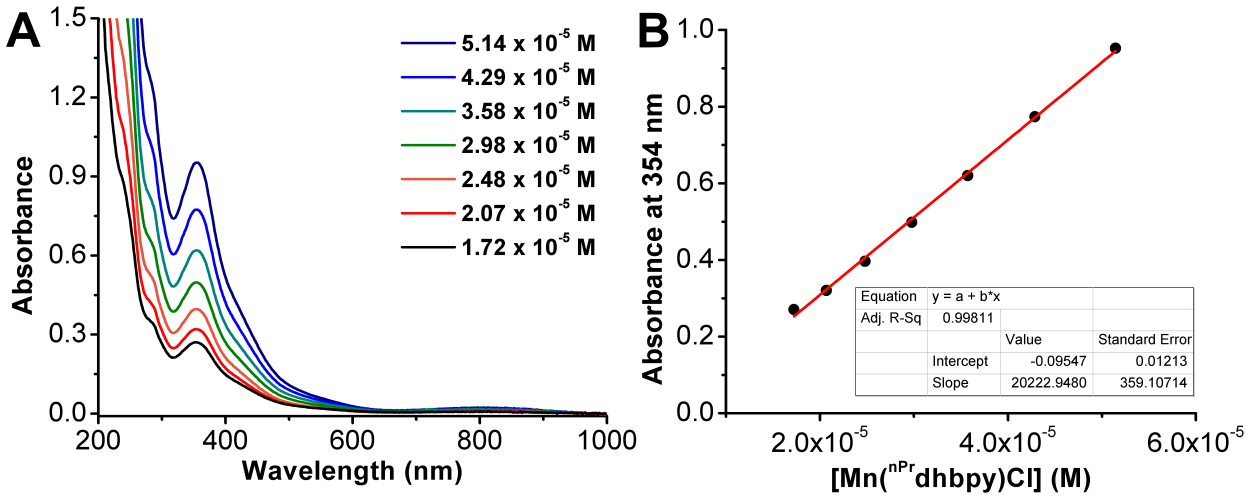

Figure S2. UV-vis serial dilution of Mn(^{nPr}dhbpy)Cl **2** in MeCN solution. Conditions: varying concentration; 1 cm pathlength (B) plot of concentration of Mn(^{nPr}dhbpy)Cl (M) versus absorbance at 356 nm (20223 M^{-1} cm^{-1}), R^2 = 0.998. All: 288 nm (25576 M^{-1}cm^{-1}), 440 nm (7626 M^{-1}cm^{-1}), 540 nm (1447 M^{-1}cm^{-1}), 802 nm (496 M^{-1}cm^{-1}).

Table S2. Table of Evans' Method data from Mn(^{nPr}dhbpy)Cl **2** in *N,N′*-DMF (chosen for solubility reasons) supporting a high spin d^4 complex.

Trial	Chemical Shift (ppm)	Chemical Shift (Hz)	Total Magnetic Moment (emu mol^{-1})	Paramagnetic Moment (emu mol^{-1})	μ_{eff} (Bohr Magnetons)
1	0.12	72	8.21×10^{-3}	8.61×10^{-3}	4.53
2	0.13	78	8.89×10^{-3}	9.29×10^{-3}	4.71
3	0.12	72	8.21×10^{-3}	8.61×10^{-3}	4.53

Synthesis of DIPEAHPF$_6$

N,N-diisopropylethylammonium hexafluorophosphate (DIPEAHPF$_6$) was synthesized according to previously reported procedures.[4] A solution of ammonium hexafluorophosphate (2.81 g, 17.2 mmol) and N,N-diisopropylethylamine (3.30 mL, 19.0 mmol) was allowed to reflux in toluene (20 mL) for 48 hours to obtain a white solid. The solution was filtered and the solid was rinsed toluene (with 2 x 10 mL). The solid was dissolved in DCM, filtered, and the solvent was removed under reduced pressure to yield a white crystalline solid in 25.5% yield (1.2 g). White x-ray suitable single crystals were grown by slow evaporation from DCM. Elemental analysis for $C_8H_{20}F_6NP$: calc'd: C 34.91, H 7.33, N 5.09; found: C 35.00, H 7.46, N 5.09. ^{1}H NMR (MeCN-d_3, 600 MHz) δ (ppm): 6.18 (t, 1H), 3.67 (sept, 2H), 3.16 (q, 2H), 1.32 (m, 15H). ^{13}C{^{1}H} (MeCN-d_3, 150 MHz) δ (ppm): 56.19, 44.13, 18.79, 17.42, 13.00.

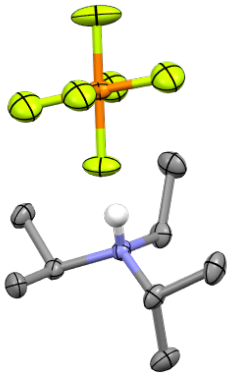

Figure S3. Molecular structure of DIPEAHPF$_6$ from single crystal X-ray diffraction studies. Blue = N, gray = C, white = H, green = F, orange; thermal ellipsoids at 50%, H atoms (except N–H) and disordered F atoms omitted for clarity. CCDC 2255850.

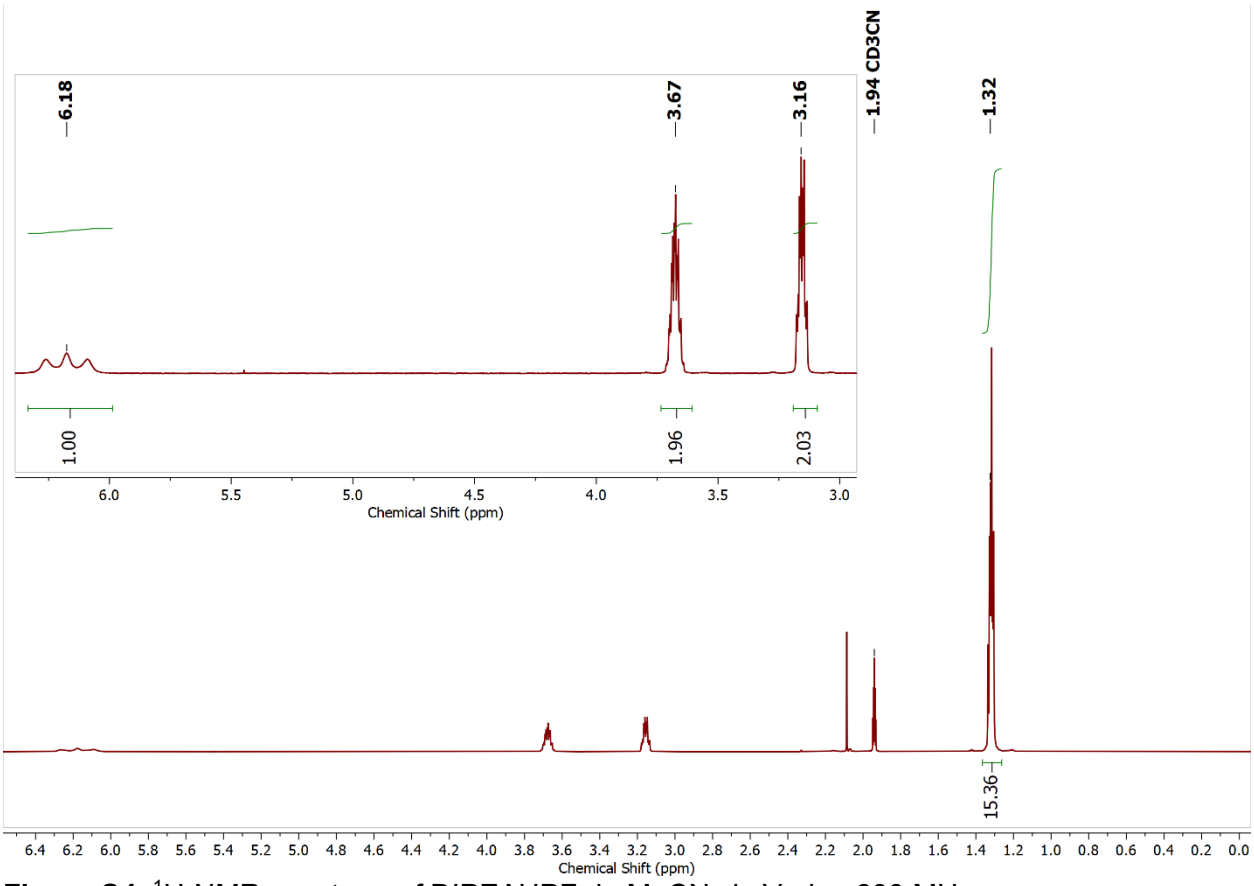

Figure S4. ^{1}H-NMR spectrum of DIPEAHPF$_6$ in MeCN-d_3; Varian 600 MHz.

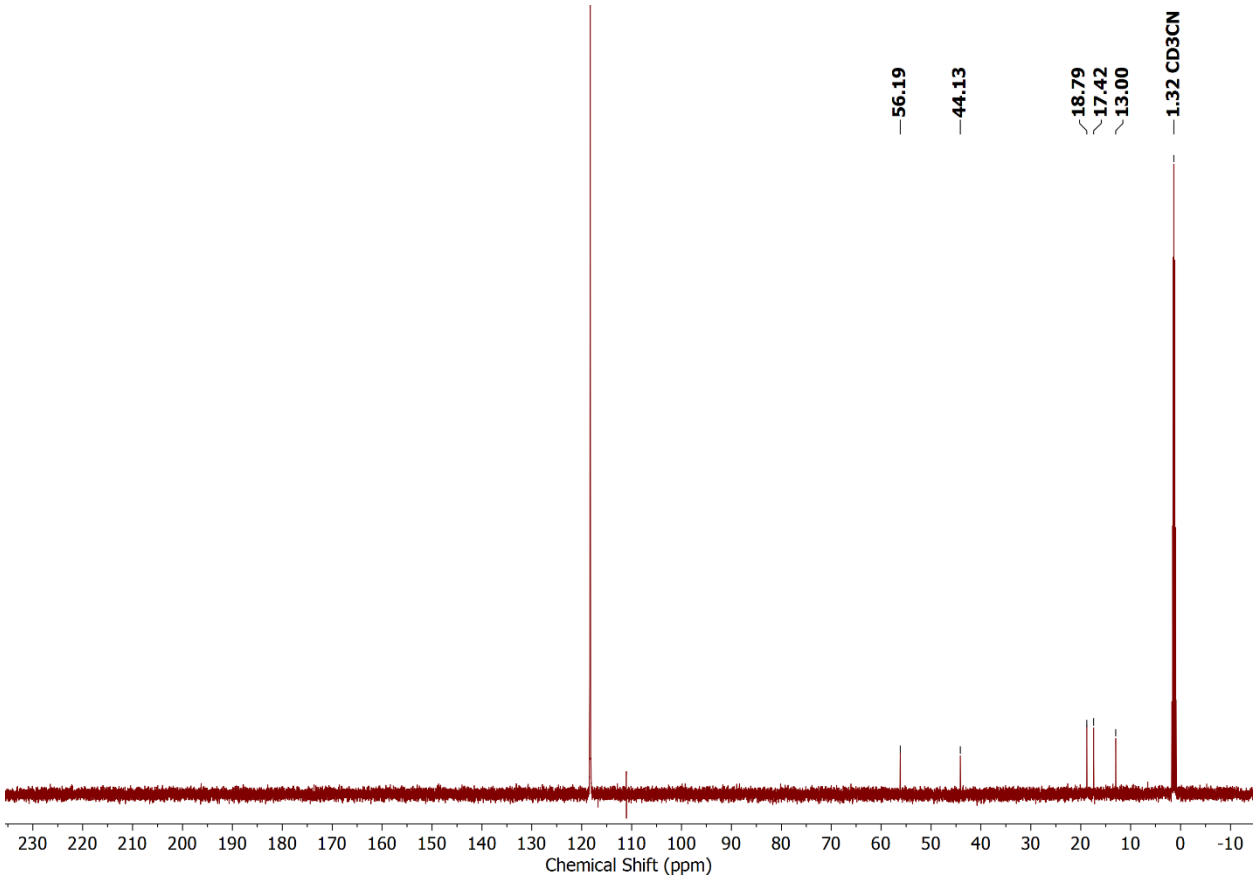

Figure S5. $^{13}C\{^{1}H\}$-NMR spectrum of DIPEAHPF$_6$ in MeCN-d_3; Varian 150 MHz.

Estimation of $DIPEAHPF_6$ pK_a in MeCN

^{1}H-NMR spectroscopy was used to estimate the pK_a of $DIPEAHPF_6$ in acetonitrile relative to triethylamine (pK_a(MeCN) = 18.81), as previously reported.[5] Triethylamine (TEA) was titrated into a solution of 0.02 M $DIPEAHPF_6$ in MeCN-d_3 and a ^{1}H-NMR spectrum was taken (**Figure S7**). The difference in chemical shift was used to determine the relative change in pK_a units according to **Eqs S1-S3**. Triethylammonium hexfluorophosphate ($TEAHPF_6$) was synthesized according to a literature procedure.[4]

$$DIPEAH^+\left(B-H_j^+\right)+TEA\ (B_i) \rightleftharpoons TEAH^+(B-H_i^+)+DIPEA\ (B_j) \qquad \textbf{Eq S1}$$

$$\frac{K_{a_i}}{K_{a_j}}=\frac{(\delta_j^{obs}-\delta_j^B)(\delta_i^{B-H^+}-\delta_i^{obs})}{(\delta_i^{obs}-\delta_i^B)(\delta_j^{B-H^+}-\delta_j^{obs})} \qquad \textbf{Eq S2}$$

$$\Delta pK_{a_{ij}}=\log\left|\frac{K_{a_i}}{K_{a_j}}\right|=0.142\ \pm 0.083 \qquad \textbf{Eq S3}$$

Table S3. Summary of the chemical shifts for the estimation of $DIPEAHPF_6$ pK_a.

TEA:DIPEAHPF$_6$	**δ^{B}_{j} (ppm)**	**δ^{obs}_{j} (ppm)**	**$\delta^{B\text{-}H^+}_{j}$ (ppm)**	**δ^{B}_{i} (ppm)**	**δ^{obs}_{i} (ppm)**	**$\delta^{B\text{-}H^+}_{i}$ (ppm)**	**K_{ai}/K_{aj}**	**$\log\lvert K_{ai}/K_{aj}\rvert$**
0.10	3.01	3.63	3.68	2.46	3.07	3.14	–1.42	0.153
0.20		3.58			3.03		–1.10	0.0414
0.35		3.53			2.96		–1.25	0.0962
0.49		3.48			2.91		–1.20	0.0800
0.64		3.45			2.87		–1.26	0.100
0.79		3.42			2.84		–1.24	0.0951
0.94		3.39			2.81		–1.24	0.0918
1.1		3.31			2.71		–1.39	0.144
5.7		3.12			2.55		–1.29	0.110
11		3.06			2.5		–1.29	0.111
18		3.05			2.49		–1.38	0.139
20		3.05			2.48		–2.10	0.321
23		3.04			2.48		–1.55	0.190
25		3.03			2.47		–2.06	0.314
							Average	0.142
							Standard Deviation	0.083

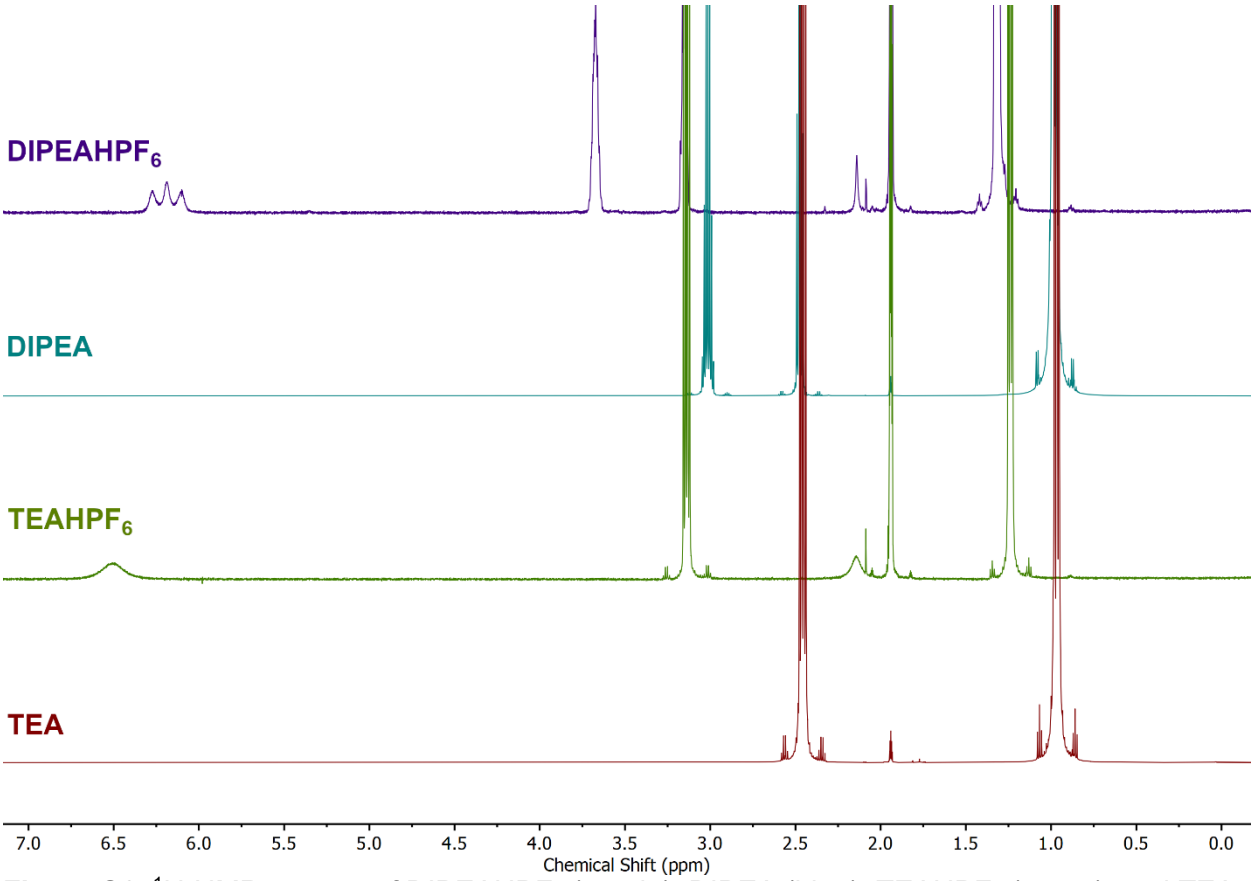

Figure S6. ^{1}H-NMR spectra of DIPEAHPF$_6$ (purple), DIPEA (blue), TEAHPF$_6$ (green), and TEA (red) used to estimate the pK_a of DIPEAHPF$_6$ in MeCN. MeCN-d_3; Varian 600 MHz.

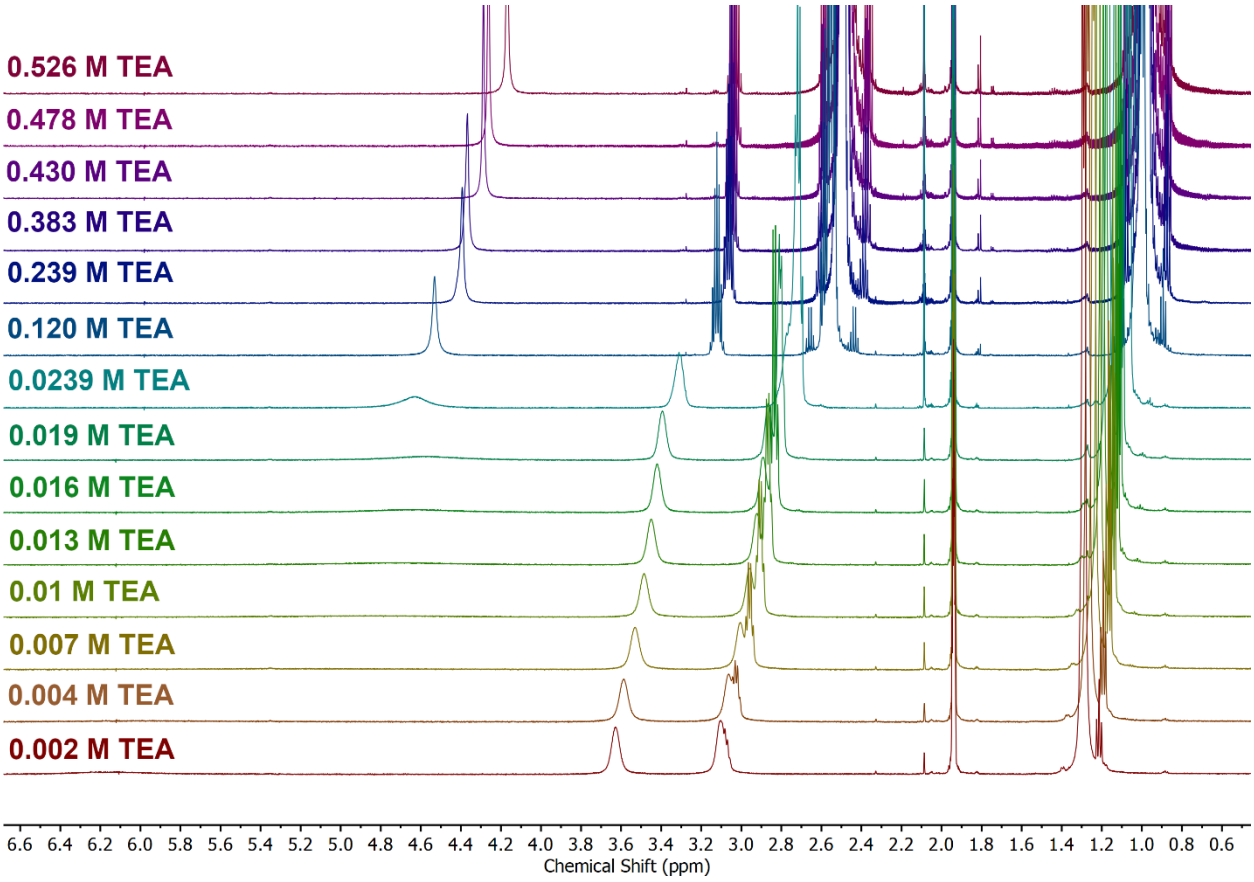

Figure S7. ^{1}H NMR of titration of TEA into a 0.02 M solution of DIPEAHPF$_6$ for estimation of pK_a of DIPEAHPF$_6$ in MeCN. MeCN-d_3; Varian 600 MHz.

Electrochemical Analysis

All electroanalytical experiments were performed using a Metrohm Autolab PGSTAT302N potentiostat. Glassy carbon working (⌀ = 3 mm) and non-aqueous silver/silver chloride pseudoreference electrodes behind PTFE tips were obtained from CH Instruments. The pseudoreference electrodes were obtained by depositing chloride on bare silver wire in 10% HCl at oxidizing potentials and stored in a 0.1 M tetrabutylammonium hexafluorophosphate solution in acetonitrile in the dark prior to use. The counter electrode was a glassy carbon rod (⌀ = 3 mm). All CV experiments were performed in a modified scintillation vial (20 mL volume) as a single-chamber cell with a cap modified with ports for all electrodes and a sparging needle. Tetrabutylammonium hexafluorophosphate ($TBAPF_6$) was purified by recrystallization from ethanol and dried in a vacuum oven before being stored in a desiccator. All data were referenced to an internal ferrocene standard (ferrocenium/ferrocene reduction potential under stated conditions) unless otherwise specified. All voltammograms were corrected for internal resistance. Ferrocene was purified by sublimation prior to use. In the event that the presence of electrochemical features precluded ferrocene addition, ferrocene was added to the electrochemical cell at the end of analysis for reference.

Electrochemistry with 1

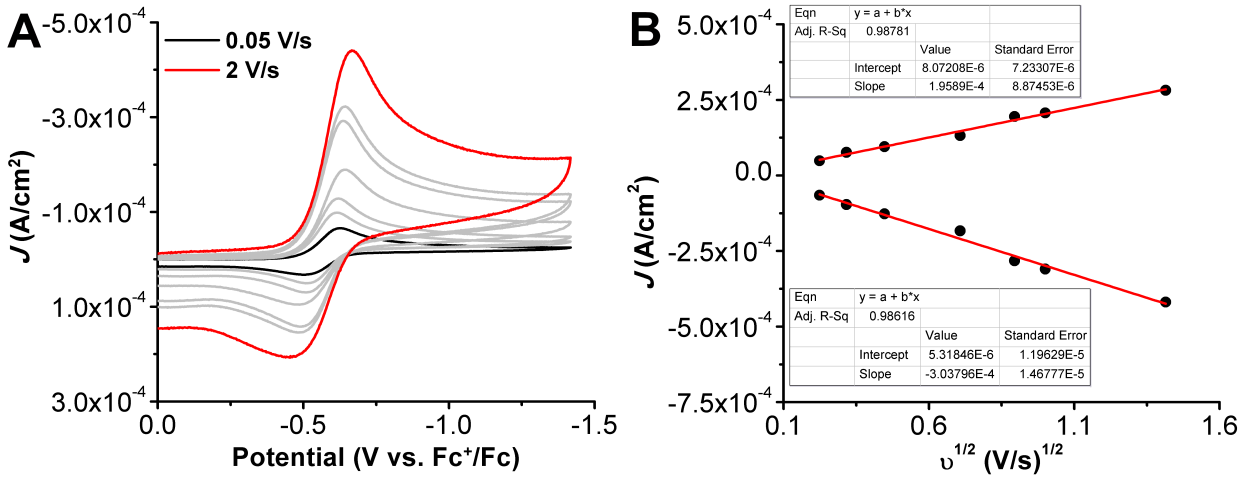

Figure S8. (A) CVs of Mn($^{p\text{-tbu}}$dhbpy)Cl **1** at variable scan rates ranging from 0.05 V/s (black) to 2 V/s (red) under Ar saturation conditions. (B) Linear fit data from A showing that Mn($^{p\text{-tbu}}$dhbpy)Cl is a diffusion-limited current response. Conditions: 0.5 mM Mn, 0.1 M $TBAPF_6$/MeCN; glassy carbon working electrode, glassy carbon rod counter electrode, Ag/AgCl pseudoreference electrode; referenced to Fc^+/Fc internal standard; 100 mV/s scan rate.

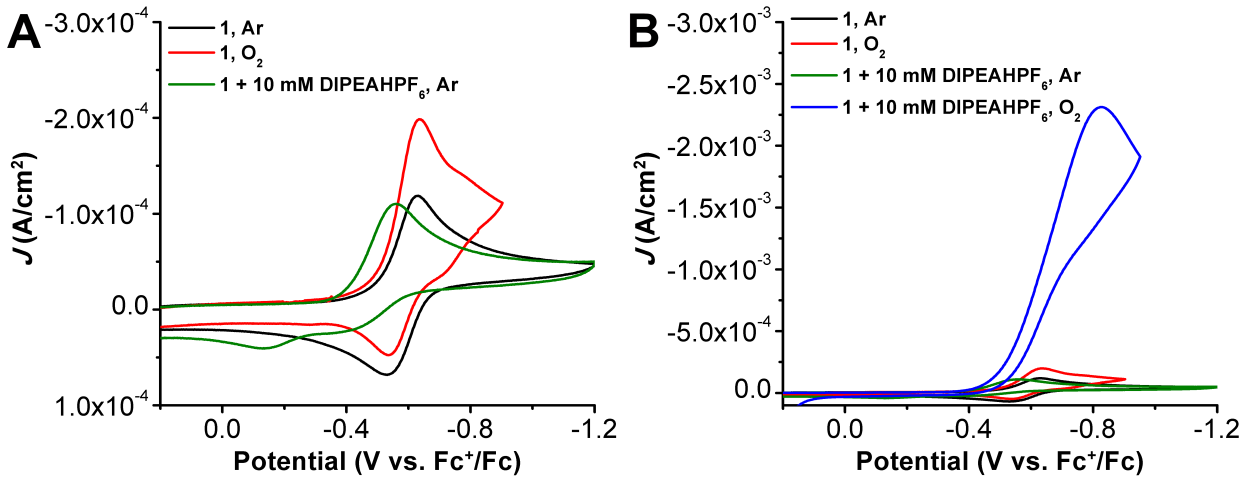

Figure S9. (A) CVs of Mn($^{p\text{-tbu}}$dhbpy)Cl **1** under Ar (black), O_2 (red) and with 10 mM $DIPEAHPF_6$ under Ar saturation (green). (B) CVs from A and catalytic trace shown (blue) with Mn($^{p\text{-tbu}}$dhbpy)Cl 1 and 10 mM $DIPEAHPF_6$ under O_2 saturation. Conditions: 0.5 mM Mn, 0.1 M $TBAPF_6$/MeCN; glassy carbon working electrode, glassy carbon rod counter electrode, Ag/AgCl pseudoreference electrode; referenced to Fc^+/Fc internal standard; 100 mV/s scan rate.

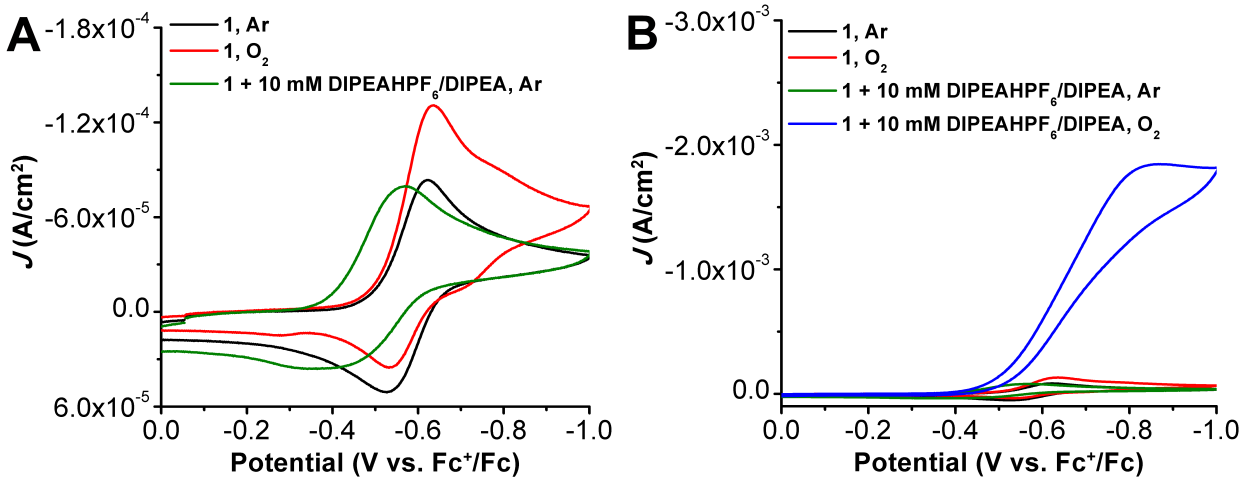

Figure S10. (A) CVs of Mn($^{p\text{-tbu}}$dhbpy)Cl **1** under Ar (black), O_2 (red) and with 10 mM buffer ($DIPEAHPF_6$/DIPEA) under Ar saturation (green). (B) CVs from A with catalytic trace shown (blue) with Mn($^{p\text{-tbu}}$dhbpy)Cl and 10 mM $DIPEAHPF_6$/DIPEA under O_2 saturation. Conditions: 0.5 mM Mn, 0.1 M $TBAPF_6$/MeCN; glassy carbon working electrode, glassy carbon rod counter electrode, Ag/AgCl pseudoreference electrode; referenced to Fc^+/Fc internal standard; 100 mV/s scan rate.

Determination of Effective Overpotential of 1

Utilizing the estimated pK_a of $DIPEAHPF_6$ (18.7) in MeCN, we can determine the effective overpotential according to **Eqs S4-S5**. Where E_{app} is the $E_{1/2}$ of Mn($^{p\text{-tbu}}$dhbpy)Cl with 10 mM $DIPEAHPF_6$ buffer determined by taking the first derivative of the irreversible feature in **Figure S10**.[6]

$$E^0_{O2/H2O} = 1.21 - 0.0592pK_a$$

$$E^0_{O2/H2O}(MeCN, DIPEAHPF_6) = 0.10\,V\ vs.\,Fc^+/Fc \qquad \textbf{Eq S4}$$

$$\eta = \left|E_{app} - E^0_{O2/H2O}\right| = |-0.48 - 0.10| = 0.58\,V \qquad \textbf{Eq S5}$$

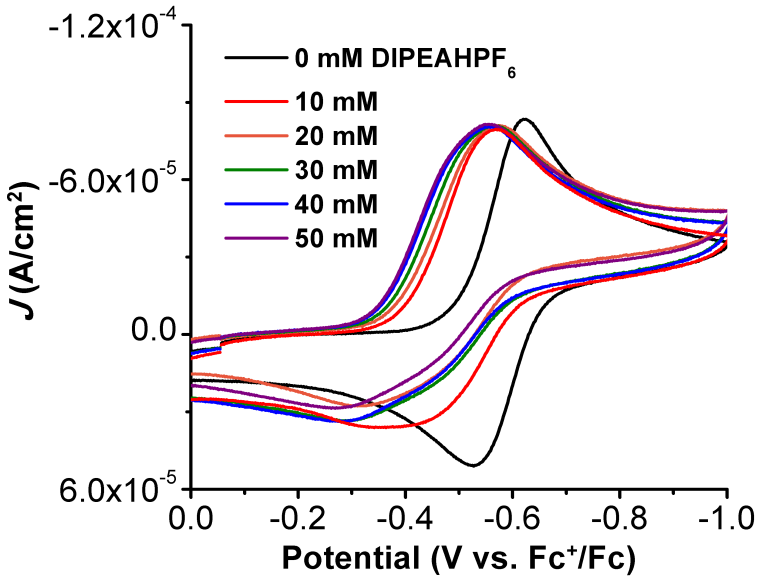

Figure S11. CVs of Mn($^{p\text{-tbu}}$dhbpy)Cl **1** with increasing $DIPEAHPF_6$ concentrations under Ar saturation conditions with 10 mM DIPEA. Conditions: 0.5 mM Mn, 10 mM DIPEA, 0.1 M $TBAPF_6$/MeCN; glassy carbon working electrode, glassy carbon rod counter electrode, Ag/AgCl pseudoreference electrode; referenced to Fc^+/Fc internal standard; 100 mV/s scan rate.

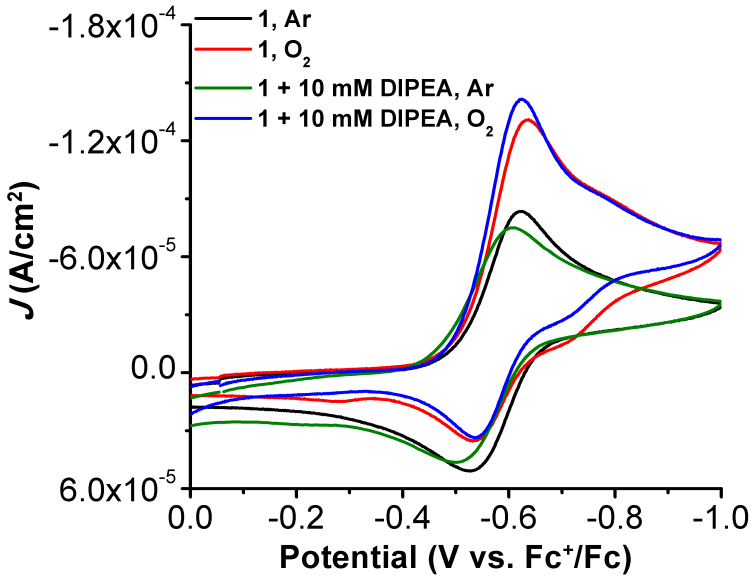

Figure S12. Control CVs of Mn($^{p\text{-tbu}}$dhbpy)Cl **1** with and without the presence of 10 mM DIPEA. Conditions: 0.5 mM Mn, 10 mM DIPEA, 0.1 M $TBAPF_6$/MeCN; glassy carbon working electrode, glassy carbon rod counter electrode, Ag/AgCl pseudoreference electrode; referenced to Fc^+/Fc internal standard; 100 mV/s scan rate.

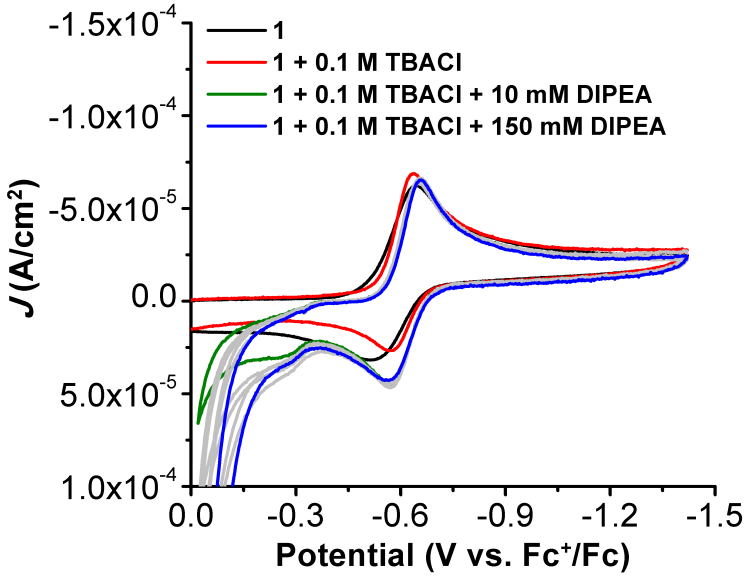

Figure S13. CVs of Mn($^{p\text{-tbu}}$dhbpy)Cl **1** (black trace) in the presence of 0.1 M TBACl (red trace) with increasing concentrations of DIPEA added. Conditions: 0.3 mM Mn, 0.1 M TBACl (if present), [DIPEA]: 10 mM (green trace), 20 mM, 30 mM, 50 mM, 100 mM, 150 mM (blue trace), 0.1 M $TBAPF_6$/MeCN; glassy carbon working electrode, glassy carbon rod counter electrode, Ag/AgCl pseudoreference electrode; referenced to Fc^+/Fc internal standard; 100 mV/s scan rate.

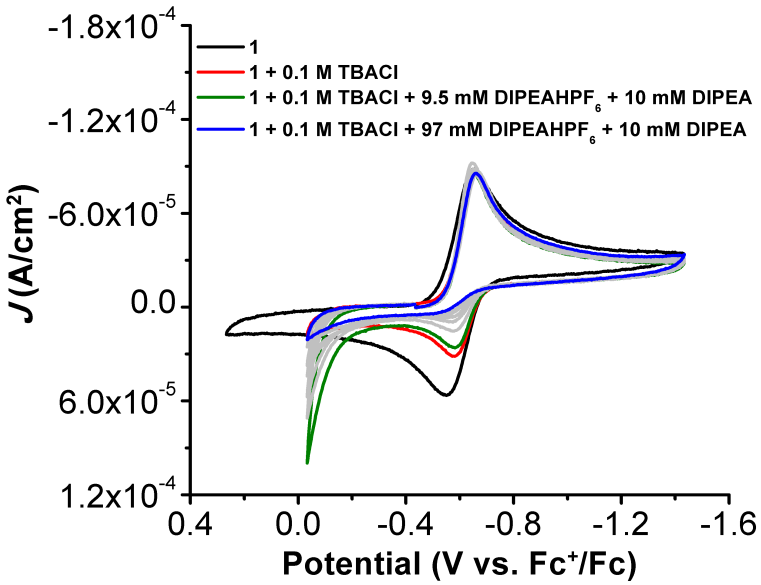

Figure S14. CVs of Mn($^{p\text{-}tbu}$dhbpy)Cl **1** (black trace) in the presence of 0.1 M TBACl (red trace) and 10 mM DIPEA with increasing concentrations of $DIPEAHPF_6$ under Ar saturation. Conditions: 0.3 mM Mn, 0.1 M TBACl (if present), 10 mM DIPEA (if present), 0.1 M $TBAPF_6$/MeCN; glassy carbon working electrode, glassy carbon rod counter electrode, Ag/AgCl pseudoreference electrode; referenced to Fc^+/Fc internal standard; 100 mV/s scan rate. Concentration of $DIPEAHPF_6$: 9.5 (green trace), 18.9, 29.2, 38.5, 47.8, 57.8, 97 mM (blue trace).

Electrochemistry with 2

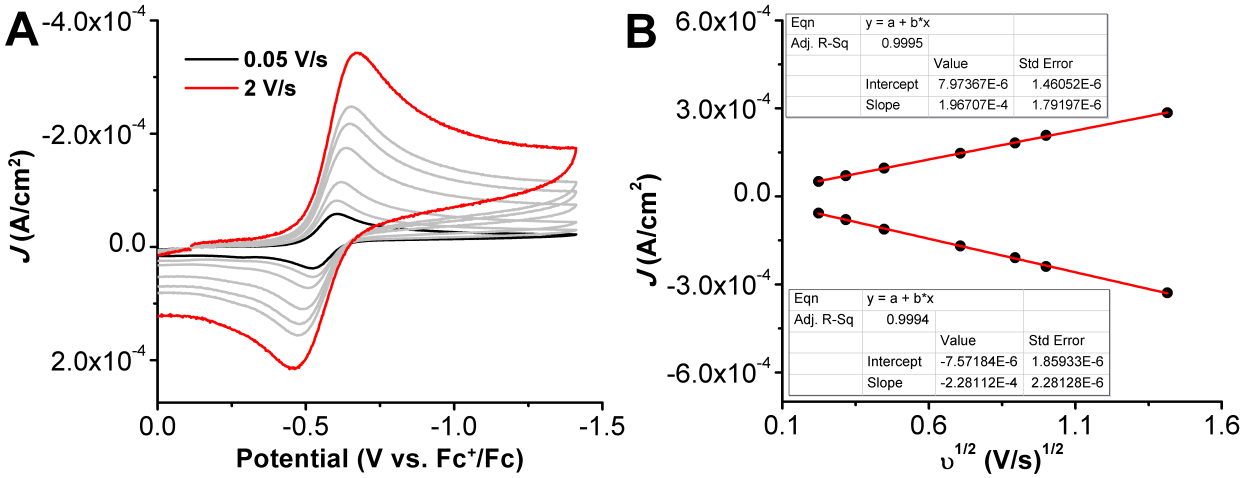

Figure S15. A) CVs of Mn(^{nPr}dhbpy)Cl **2** at variable scan rates ranging from 0.05 V/s (black) to 2 V/s (red) under Ar saturation conditions. (B) Linear fit data from A showing that Mn(^{nPr}dhbpy)Cl is a diffusion-limited current response. Conditions: 0.5 mM Mn, 0.1 M $TBAPF_6$/MeCN; glassy carbon working electrode, glassy carbon rod counter electrode, Ag/AgCl pseudoreference electrode; referenced to Fc^+/Fc internal standard; 100 mV/s scan rate.

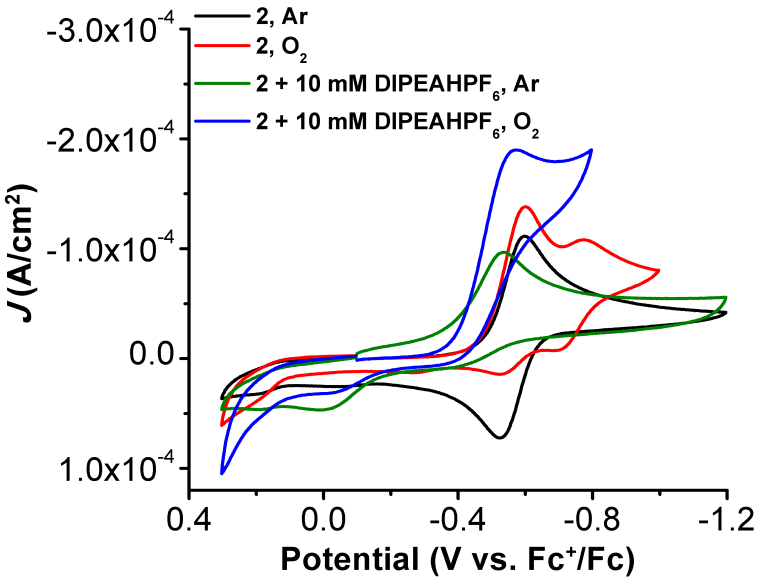

Figure S16. CVs of Mn(^{nPr}dhbpy)Cl **2** under Ar (black), O_2 (red) and with 10 mM DIPEAHPF$_6$ under Ar saturation (green). Conditions: 0.5 mM Mn, 0.1 M TBAPF$_6$/MeCN; glassy carbon working electrode, glassy carbon rod counter electrode, Ag/AgCl pseudoreference electrode; referenced to Fc^+/Fc internal standard; 100 mV/s scan rate.

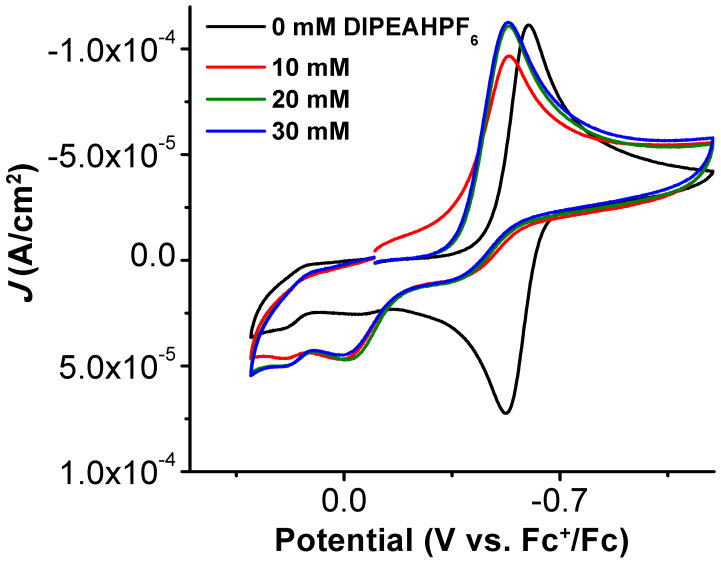

Figure S17. (A) CVs of Mn(^{nPr}dhbpy)Cl **2** under Ar with increasing amounts of DIPEAHPF$_6$ added. Conditions: 0.5 mM Mn, 0.1 M TBAPF$_6$/MeCN; glassy carbon working electrode, glassy carbon rod counter electrode, Ag/AgCl pseudoreference electrode; referenced to Fc^+/Fc internal standard; 100 mV/s scan rate.

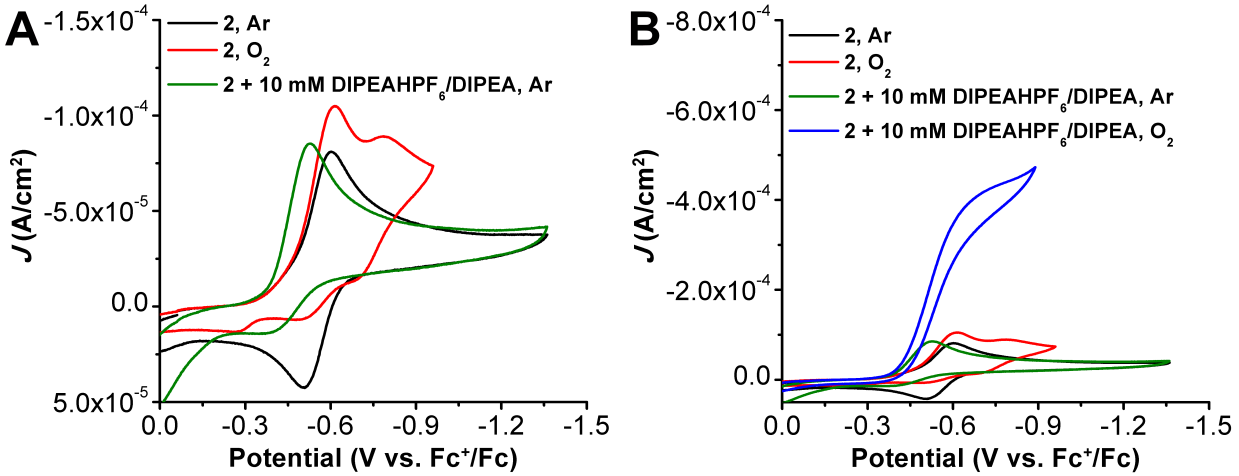

Figure S18. (A) CVs of Mn(^{nPr}dhbpy)Cl **2** under Ar (black), O_2 (red) and with 10 mM $DIPEAHPF_6$/DIPEA under Ar saturation (green). (B) CVs from A with catalytic trace shown (blue) with Mn(^{nPr}dhbpy)Cl and 10 mM $DIPEAHPF_6$/DIPEA under O_2 saturation. Conditions: 0.5 mM Mn, 0.1 M $TBAPF_6$/MeCN; glassy carbon working electrode, glassy carbon rod counter electrode, Ag/AgCl pseudoreference electrode; referenced to Fc^+/Fc internal standard; 100 mV/s scan rate.

Determination of Effective Overpotential of 2

Utilizing the estimated pK_a of $DIPEAHPF_6$ (18.7) in MeCN, we can determine the effective overpotential according to **Eqs S6-S7**. Where E_{app} is the $E_{1/2}$ of Mn(^{nPr}dhbpy)Cl **2** with 10 mM $DIPEAHPF_6$ buffer determined by taking the first derivative of the irreversible feature in **Figure S18**.[6]

$$E^0_{O2/H2O} = 1.21 - 0.0592pK_a$$

$$E^0_{O2/H2O}(MeCN, DIPEAHPF_6) = 0.10\ V\ vs.\ Fc^+/Fc \qquad \textbf{Eq S6}$$

$$\eta = \left|E_{app} - E^0_{O2/H2O}\right| = |-0.46 - 0.10| = 0.56\ V \qquad \textbf{Eq S7}$$

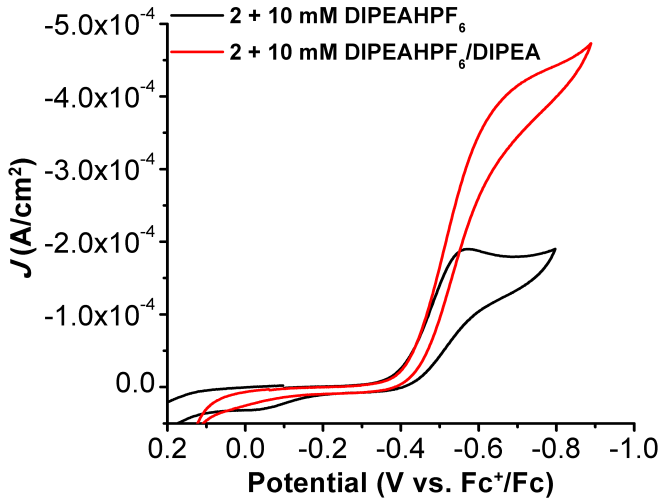

Figure S19. Comparison of electrocatalytic ORR by Mn(^{nPr}dhbpy)Cl **2** with 10 mM DIPEAHPF$_6$ with (red) and without (black) the presence of 10 mM DIPEA (traces from **Figure S16** and **S18** for black and red traces, respectively). Conditions: 0.5 mM Mn, 0.1 M TBAPF$_6$/MeCN; glassy carbon working electrode, glassy carbon rod counter electrode, Ag/AgCl pseudoreference electrode; referenced to Fc$^+$/Fc internal standard; 100 mV/s scan rate.

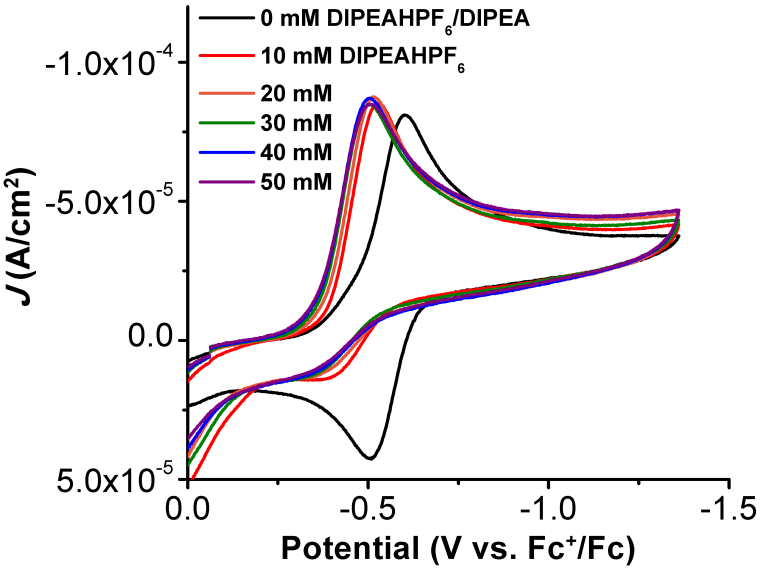

Figure S20. CVs of Mn(^{nPr}dhbpy)Cl **2** with increasing DIPEAHPF$_6$ concentrations under Ar saturation conditions with 10 mM DIPEA. Conditions: 0.5 mM Mn, 10 mM DIPEA, 0.1 M TBAPF$_6$/MeCN; glassy carbon working electrode, glassy carbon rod counter electrode, Ag/AgCl pseudoreference electrode; referenced to Fc$^+$/Fc internal standard; 100 mV/s scan rate.

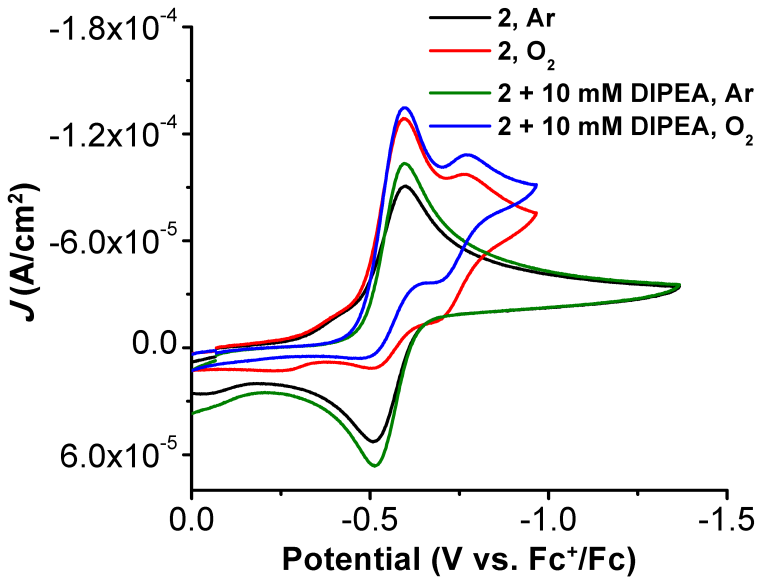

Figure S21. Control CVs of Mn(^{nPr}dhbpy)Cl **2** with and without the presence of 10 mM DIPEA. Conditions: 0.5 mM Mn, 10 mM DIPEA, 0.1 M $TBAPF_6$/MeCN; glassy carbon working electrode, glassy carbon rod counter electrode, Ag/AgCl pseudoreference electrode; referenced to Fc^+/Fc internal standard; 100 mV/s scan rate.

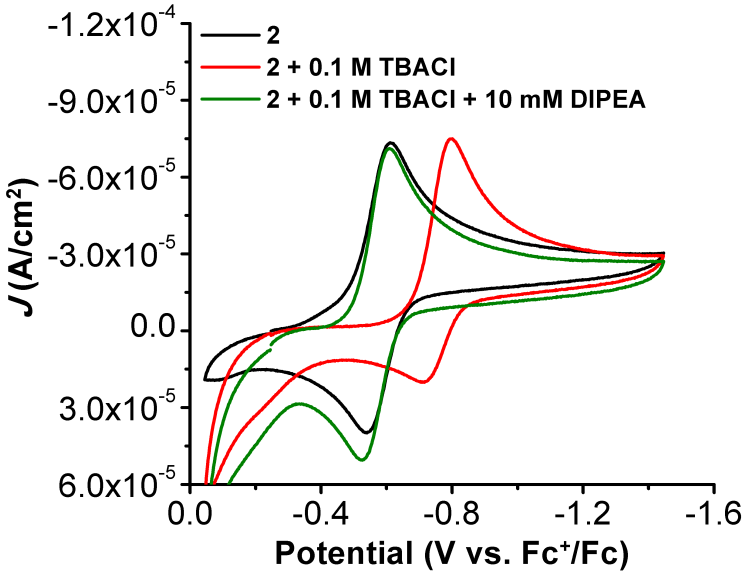

Figure S22. CVs of Mn(^{nPr}dhbpy)Cl **2** (black trace) in the presence of 0.1 M TBACl (red trace) and DIPEA (green trace). Conditions: 0.3 mM Mn, 0.1 M $TBAPF_6$/MeCN; glassy carbon working electrode, glassy carbon rod counter electrode, Ag/AgCl pseudoreference electrode; referenced to Fc^+/Fc internal standard; 100 mV/s scan rate.

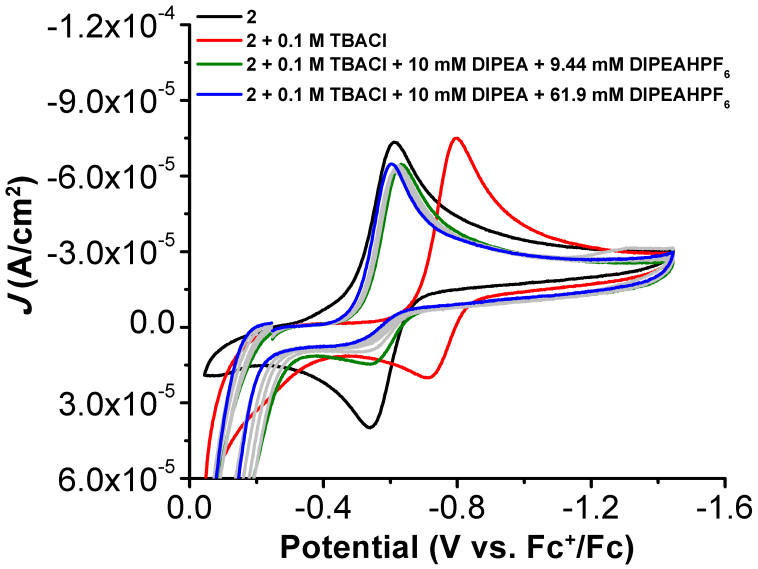

Figure S23. CVs of Mn(^{nPr}dhbpy)Cl **2** (black trace) in the presence of 0.1 M TBACl (red trace) and increasing amounts of $DIPEAHPF_6$. Conditions: 0.3 mM Mn, 10 mM DIPEA (if present), 0.1 M $TBAPF_6$/MeCN; glassy carbon working electrode, glassy carbon rod counter electrode, Ag/AgCl pseudoreference electrode; referenced to Fc^+/Fc internal standard; 100 mV/s scan rate. Concentrations of $DIPEAHPF_6$: 9.44 (green trace), 19.1, 29.3, 39.2, 51.7, 61.9 mM (blue trace).

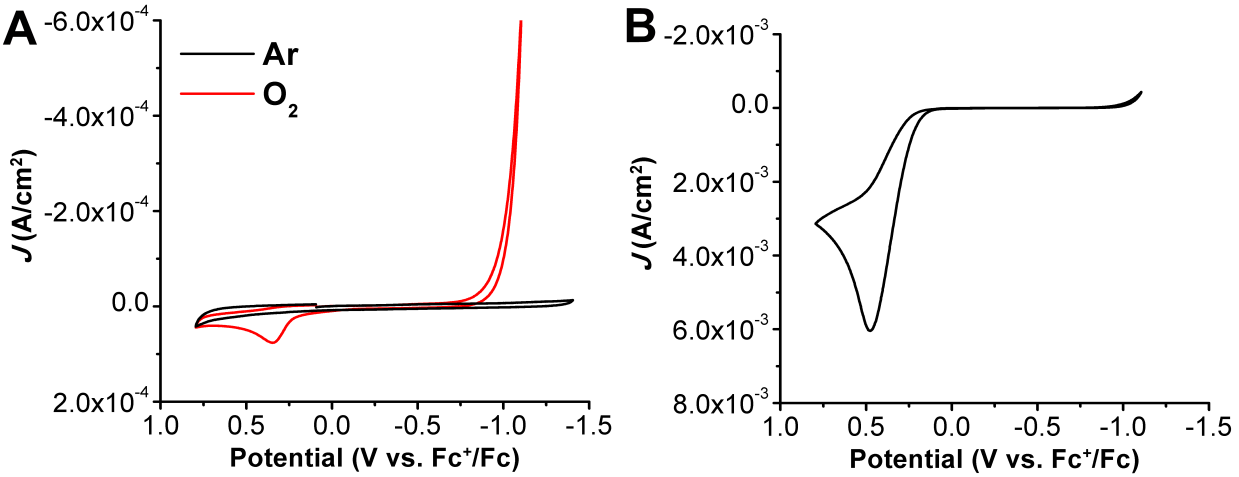

Figure S24. (A) Control CVs of 24 mM $DIPEAHPF_6$ under Ar (black) and O_2 (red trace). (B) Control CVs of 24 mM $DIPEAHPF_6$ and 25 mM DIPEA under O_2. Conditions: 24 mM $DIPEAHPF_6$, 0.1 M $TBAPF_6$/MeCN; glassy carbon working electrode, glassy carbon rod counter electrode, Ag/AgCl pseudoreference electrode; referenced to Fc^+/Fc internal standard; 100 mV/s scan rate.

Description of Spectrochemical ORR Product Quantification

The concentration of catalytically produced H_2O_2 was determined by $Ti(O)SO_4$ as previously reported.[7] A calibration curve (**Figure S25**) was obtained through a serial dilution of a stock solution of urea•H_2O_2 in MeCN. H_2O_2 was extracted by adding 2 mL of a standard solution to 10 mL DCM and 5 mL of DI H_2O, inverted and allowed to separate. Then, 3 mL of the aqueous layer was removed and put into the cuvette where a UV-vis spectrum was taken before and after the addition of 0.1 mL of $Ti(O)SO_4$ solution. The difference in absorbance at 408 nm was used to construct the calibration curve (**Figure S25**).

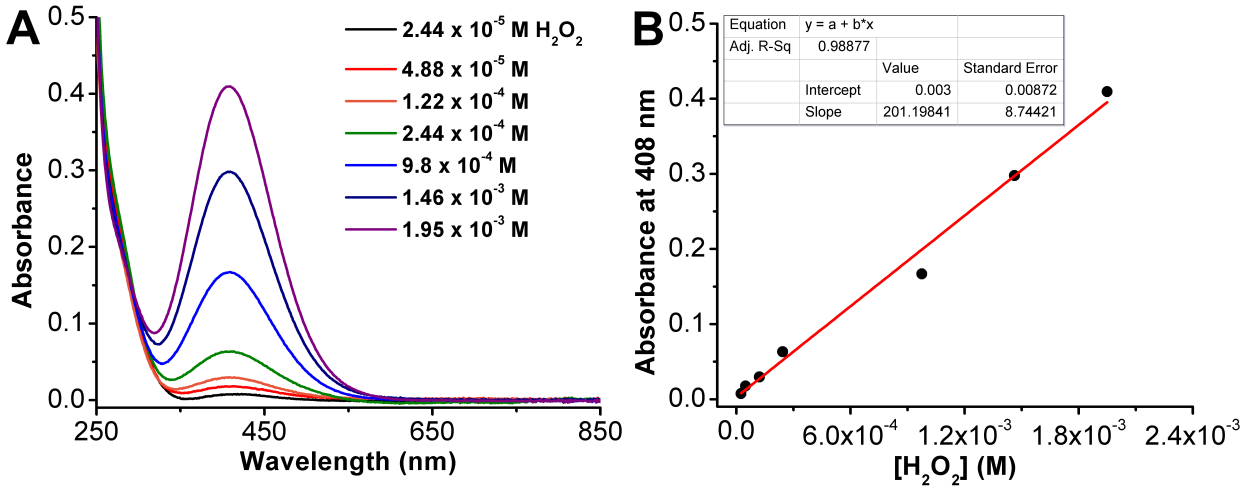

Figure S25. Calibration curve of H_2O_2 quantification using a $Ti(O)SO_4$ colorimetric assay. (A) Serial dilution of urea•H_2O_2 using the method described above. (B) Calibration curve made from data in A.

Generally, to determine the ORR selectivity of Mn(^{nPr}dhbpy)Cl **1** and Mn($^{p\text{-}tbu}$dhbpy)Cl **2**, solutions containing 80 µM [Mn] and 20 mM $DIPEAHPF_6$ and DIPEA (if present) were sparged with O_2 gas and rapidly mixed in a 1:1 ratio with a N_2 saturated 2 mM Cp^*_2Fe solution with a final volume of 8 mL (final concentrations: 40 µM Mn, 1 mM Cp^*_2Fe, 10 mM $DIPEAHPF_6$ and 10 mM DIPEA). Over the course of the reaction, 2 mL aliquots of the catalytic solution were removed and extracted with 10 mL of DCM and 5 mL of DI H_2O. The aqueous layer (3 mL) was removed and put into the cuvette and a UV-vis spectrum was taken before and after the addition of 0.1 mL of $Ti(O)SO_4$. Aliquots were taken at the indicated time points and experiments were done in triplicate. **Eqs S8-S9** were used to calculate the % selectivity of H_2O_2.

$$O_2 + 2Cp^*_2Fe(1\ mM) + 2DIPEAHPF_6 \xrightarrow{cat.[Mn]} H_2O_2(0.5\ mM) + 2[Cp^*_2Fe]^+ + 2DIPEA \quad \textbf{Eq S8}$$

Abs@408 nm (red trace) – Abs@408 nm (black trace) = $201.2[H_2O_2]_{exp} + 0.003$

$$\frac{[H_2O_2]_{exp}}{0.5\ mM\ H_2O_2} \times 100 = \%\ H_2O_2\ selectivity \qquad \textbf{Eq S9}$$

Unbuffered Conditions

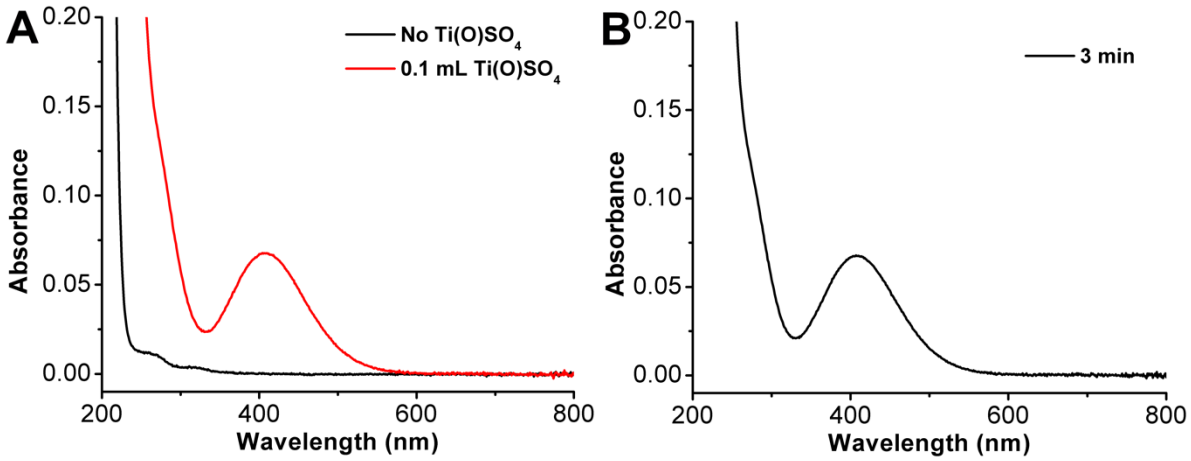

Figure S26. H_2O_2 product quantification of ORR by Mn($^{p\text{-}tbu}$dhbpy)Cl **1** with DIPEAHPF$_6$. (A) UV-vis spectrum of extracted solution after 3 min of reaction time before (black) and after (red) 0.1 mL of 0.1 M Ti(O)SO$_4$ solution was added. (B) Corrected spectra (red – black trace from A). Conditions: 40 μM Mn($^{p\text{-}tbu}$dhbpy)Cl, 10 mM DIPEAHPF$_6$, 1 mM Cp*$_2$Fe, 4.05 mM O_2 in MeCN.

Table S4. Summary of H_2O_2 selectivity of ORR by Mn($^{p\text{-}tbu}$dhbpy)Cl **1** with 10 mM DIPEAHPF$_6$ (**Figure S26**).

Time (min)	% H_2O_2	% H_2O
3	64.2 ± 6.9	35.8 ± 6.9

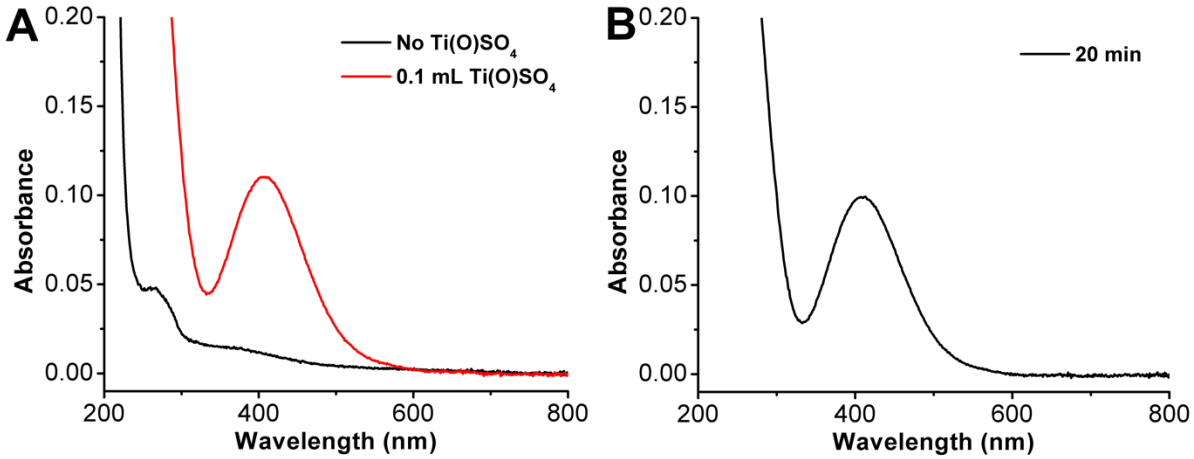

Figure S27. H_2O_2 product quantification of ORR by Mn(^{nPr}dhbpy)Cl **2** with DIPEAHPF$_6$. (A) UV-vis spectrum of extracted solution before (black) and after (red) 0.1 mL of 0.1 M Ti(O)SO$_4$ solution was added, 20 min. (B) Corrected spectra (red – black trace from A). Conditions: 40 μM Mn(^{nPr}dhbpy)Cl, 10 mM DIPEAHPF$_6$/DIPEA, 1 mM Cp*$_2$Fe, 4.05 mM O_2 in MeCN.

Table S5. Summary of H_2O_2 selectivity of ORR by Mn(^{nPr}dhbpy)Cl **2** with 10 mM DIPEAHPF$_6$ (**Figure S27**).

Time (min)	% H_2O_2	% H_2O
20	96.2 ± 4.1	3.8 ± 4.1

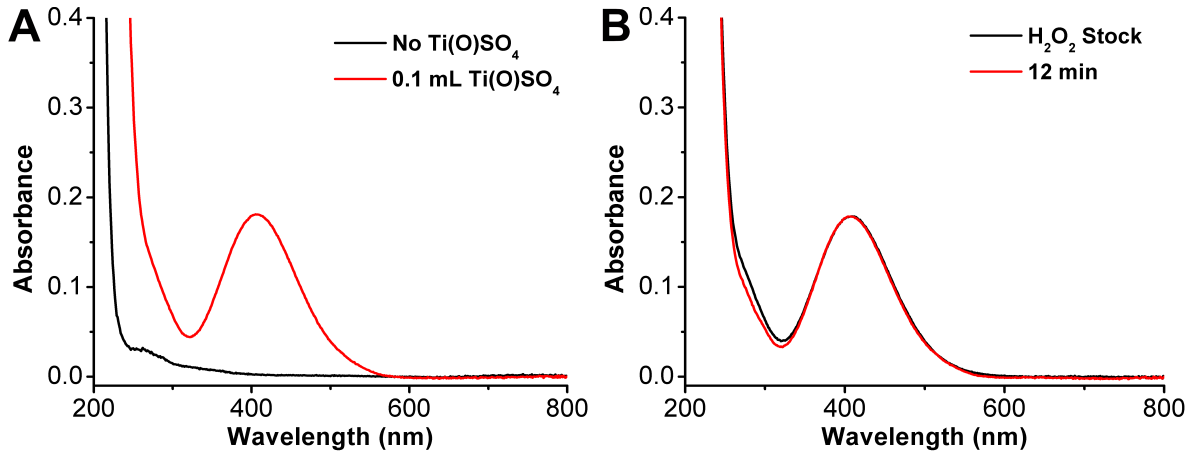

Figure S28. Stability test of urea•H_2O_2 in the presence of Mn($^{p\text{-}tbu}$dhbpy)Cl **1**, DIPEAHPF$_6$, and O_2. (A) UV-vis spectra of an extracted sample after 12 minutes of reaction time before (black) and after (red) the addition of 0.1 mL of 0.1 M Ti(O)SO$_4$. (B) Corrected UV-vis spectra (red – black trace from A) of H_2O_2 only (black) and after 12 min (red). Conditions: 40 μM Mn($^{p\text{-}tbu}$dhbpy)Cl, 10 mM DIPEAHPF$_6$, 0.87 mM urea•H_2O_2, 4.05 mM O_2 in MeCN.

Table S6. Summary of H_2O_2 disproportionation by Mn($^{p\text{-}tbu}$dhbpy)Cl **1** with 10 mM DIPEAHPF$_6$ (**Figure S28**) relative to 0.87 mM H_2O_2 stock solution.

Time (min)	% H_2O_2 Recovered
12	104 ± 8.8

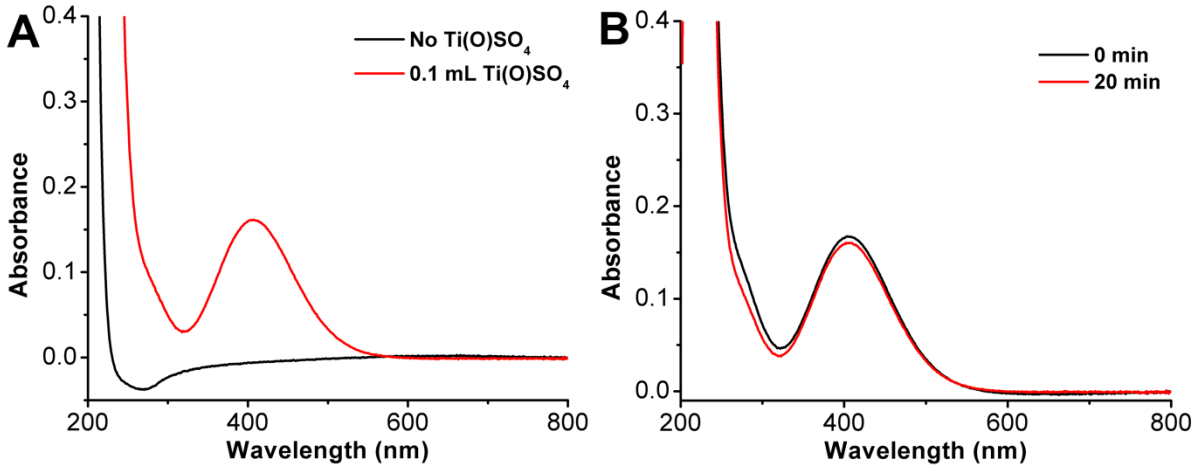

Figure S29. Stability test of urea•H_2O_2 in the presence of Mn(^{nPr}dhbpy)Cl **1**, DIPEAHPF$_6$, and O_2. (A) UV-vis spectra of an extracted sample after 20 minutes of reaction time before (black) and after (red) the addition of 0.1 mL of 0.1 M Ti(O)SO$_4$. (B) Corrected UV-vis spectra (red – black traces from A) at 0 min (black trace) and after 20 min (red). Conditions: 40 μM Mn(^{nPr}dhbpy)Cl, 10 mM DIPEAHPF$_6$, 0.80 mM urea•H_2O_2, 4.05 mM O_2 in MeCN.

Table S7. Summary of H_2O_2 disproportionation by Mn(^{nPr}dhbpy)Cl **2** with 10 mM DIPEAHPF$_6$ (**Figure S29**) relative to 0 min with 0.80 mM H_2O_2.

Time (min)	% H_2O_2 Recovered
20	93.6 ± 4.6

Buffered Conditions

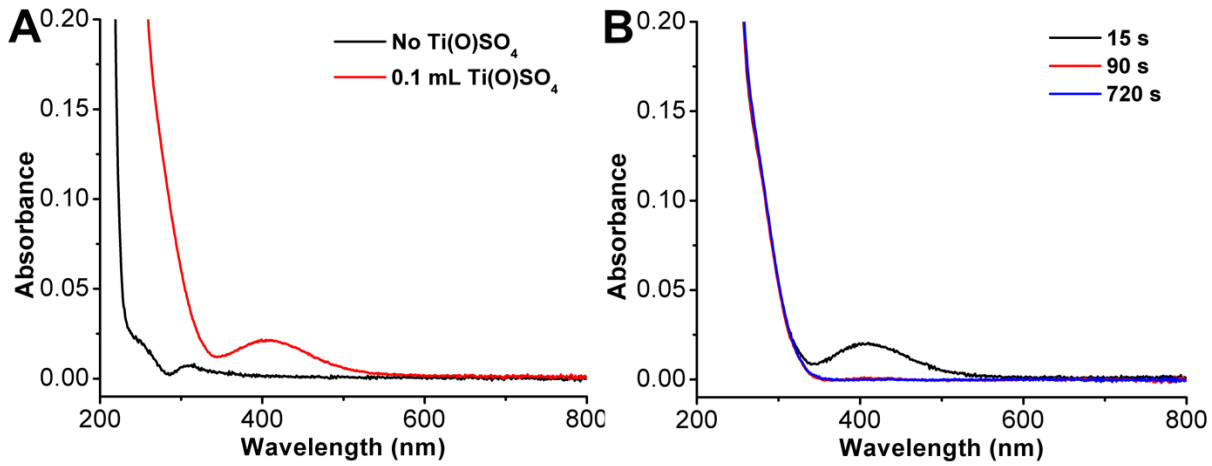

Figure S30. H_2O_2 product quantification of ORR by Mn($^{p\text{-}tbu}$dhbpy)Cl **1** with DIPEAHPF$_6$ and DIPEA. (A) UV-vis spectrum of extracted solution before (black) and after (red) 0.1 mL of 0.1 M $Ti(O)SO_4$ solution was added, 15 s. (B) Corrected spectra (red – black trace from A) for 15, 90, and 720 s aliquots. Conditions: 40 μM Mn($^{p\text{-}tbu}$dhpby)Cl, 10 mM DIPEAHPF$_6$/DIPEA, 1 mM Cp*$_2$Fe, 4.05 mM O_2 in MeCN.

Table S8. Summary of H_2O_2 selectivity over the course of catalytic ORR by Mn($^{p\text{-}tbu}$dhbpy)Cl **1** with 10 mM DIPEAHPF$_6$/DIPEA (**Figure S30**).

Time (s)	% H_2O_2	% H_2O
15	18.1 ± 4.1	81.9 ± 4.1
90	–1.32 ± 2.4	101 ± 2.4
720	–2.08 ± 1.1	102 ± 1.1

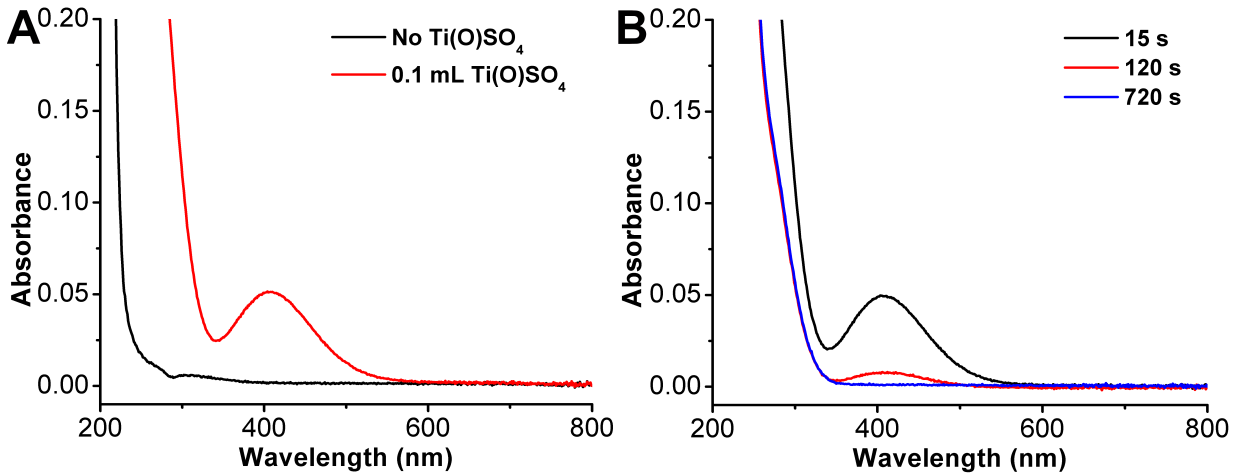

Figure S31. H_2O_2 product quantification of ORR by Mn(^{nPr}dhbpy)Cl **2** with DIPEAHPF$_6$ and DIPEA. (A) UV-vis spectra of extracted solution before (black) and after (red) 0.1 mL of 0.1 M $Ti(O)SO_4$ solution was added, 15 s. (B) Corrected spectra (red – black trace from A) for 15, 120, and 720 s aliquots. Conditions: 40 μM Mn(^{nPr}dhbpy)Cl, 10 mM DIPEAHPF$_6$/DIPEA, 1 mM Cp*$_2$Fe, 4.05 mM O_2 in MeCN.

Table S9. Summary of H_2O_2 selectivity over the course of catalytic ORR by Mn(^{nPr}dhbpy)Cl **2** with 10 mM DIPEAHPF$_6$/DIPEA (**Figure S31**).

Time (s)	% H_2O_2	% H_2O
15	37.9 ± 6.7	62.1 ± 6.7
120	6.42 ± 1.8	93.6 ± 1.8
720	-3.79 ± 1.2	103 ± 1.2

H_2O_2 Stability Testing under Buffered Conditions

To determine the stability of H_2O_2 under catalytic conditions, control studies were conducted in the presence of Mn catalyst, DIPEAHPF$_6$, DIPEA, and O_2. Generally, solutions containing 80 µM Mn catalyst and 20 mM DIPEAHPF$_6$ and DIPEA (if present) were sparged with O_2 gas and rapidly mixed in a 1:1 ratio with a N_2 saturated urea•H_2O_2 solution (final concentrations: 40 µM Mn, 10 mM DIPEAHPF$_6$ and 10 mM DIPEA). As the solution was allowed to react 2 mL aliquots were removed, extracted with 10 mL DCM and 5 mL DI H_2O. Then, 3 mL of the aqueous layer was removed and added to the cuvette. A UV-vis spectrum was taken before and after the addition of 0.1 mL of 0.1 M Ti(O)SO$_4$ solution and the difference at 408 nm was used to determine the amount of H_2O_2 present ($[H_2O_2]_{detected}$). The % recovery was determined according to **Eq S10** from measured $[H_2O_2]_{expected}$ of the H_2O_2 stock solution or time point 0 min using the described extraction method.

$$\frac{[H_2O_2]_{detected}}{[H_2O_2]_{expected}} \times 100 = \%\ H_2O_2\ recovery \qquad \textbf{Eq S10}$$

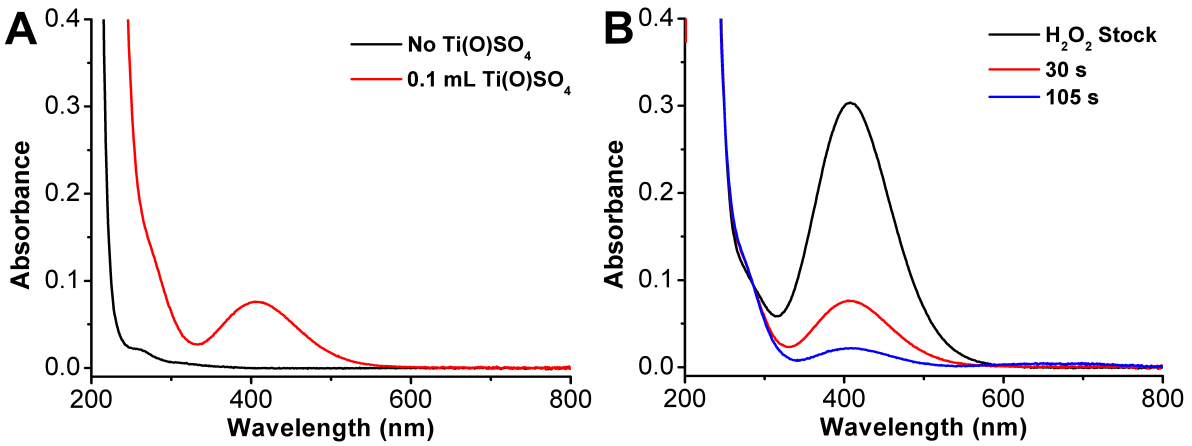

Figure S32. Stability test of urea•H_2O_2 in the presence of Mn($^{p\text{-}tbu}$dhbpy)Cl **1**, DIPEAHPF$_6$, DIPEA, and O_2. (A) UV-vis spectra before (black) and after (red) the addition of 0.1 mL of 0.1 M Ti(O)SO$_4$ to an extracted aliquot after 30 s. (B) Corrected UV-vis spectra (red – black traces) of H_2O_2 only (black) and after 30 (red) and 105 s (blue). Conditions: 40 µM Mn($^{p\text{-}tbu}$dhbpy)Cl, 10 mM DIPEAHPF$_6$/DIPEA, 1.49 mM urea•H_2O_2, 4.05 mM O_2 in MeCN.

Table S10. Summary of H_2O_2 disproportionation by Mn($^{p\text{-}tbu}$dhbpy)Cl **1** with 10 mM DIPEAHPF$_6$/DIPEA (**Figure S32**) relative to 1.49 mM H_2O_2 stock solution.

Time (s)	% H_2O_2 Recovered
30	31.3 ± 5.2
105	10.8 ± 6.6

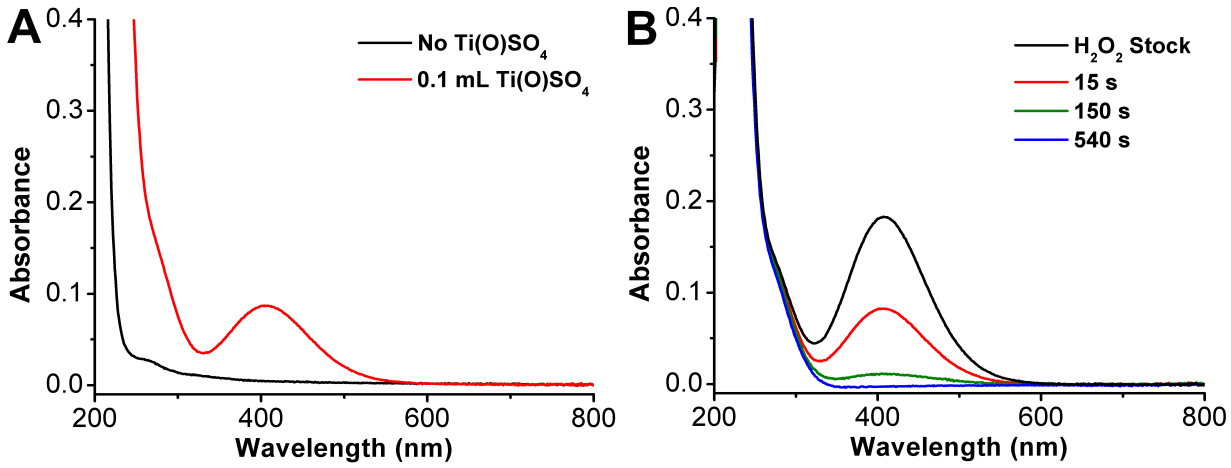

Figure S33. Stability test of urea•H_2O_2 in the presence of Mn(^{nPr}dhbpy)Cl **2**, DIPEAHPF$_6$, DIPEA, and O_2. (A) UV-vis spectra before (black) and after (red) the addition of 0.1 mL of 0.1 M Ti(O)SO$_4$ to an extracted aliquot after 15 s. (B) Corrected UV-vis spectra (red – black trace from A) of H_2O_2 only (black) and after 15 (red), 150 (green), and 540 s (blue). Conditions: 40 μM Mn(^{nPr}dhbpy)Cl, 10 mM DIPEAHPF$_6$/DIPEA, 0.89 mM urea•H_2O_2, 4.05 mM O_2 in MeCN.

Table S11. Summary of H_2O_2 disproportionation by Mn(^{nPr}dhbpy)Cl **2** with 10 mM DIPEAHPF$_6$/DIPEA (**Figure S33**) relative to 0.89 mM H_2O_2 stock solution.

Time (s)	% H_2O_2 Recovered
15	43.9 ± 4.9
150	3.81 ± 0.83
540	-3.14 ± 1.0

To determine the stability of H_2O_2 in the presence of Mn(II), control studies were conducted in the presence of Mn, DIPEAHPF$_6$, DIPEA, Cp*$_2$Fe, under an N_2 atmosphere. In a N_2 filled glovebox, urea•H_2O_2 was added to a solution containing Mn, DIPEAHPF$_6$/DIPEA, and Cp*$_2$Fe (final concentrations: 40 μM Mn, 10 mM DIPEAHPF$_6$/DIPEA, 1 mM Cp*$_2$Fe, 2.3 mM urea•H_2O_2). After 30 s, 2 min and 9 min, 2 mL aliquots were removed from the 'catalytic' solution and extracted with 10 mL of dry, degassed DCM and 5 mL of degassed water. Then, 3 mL of the aqueous layer was removed and a UV-vis spectrum was taken before and after the addition of 0.1 mL of Ti(O)SO$_4$ solution. The difference in absorbance at 408 nm was used to quantify the amount of H_2O_2 present according to **Eq S9** and **Eq S10** was used to determine the amount of H_2O_2 recovered.

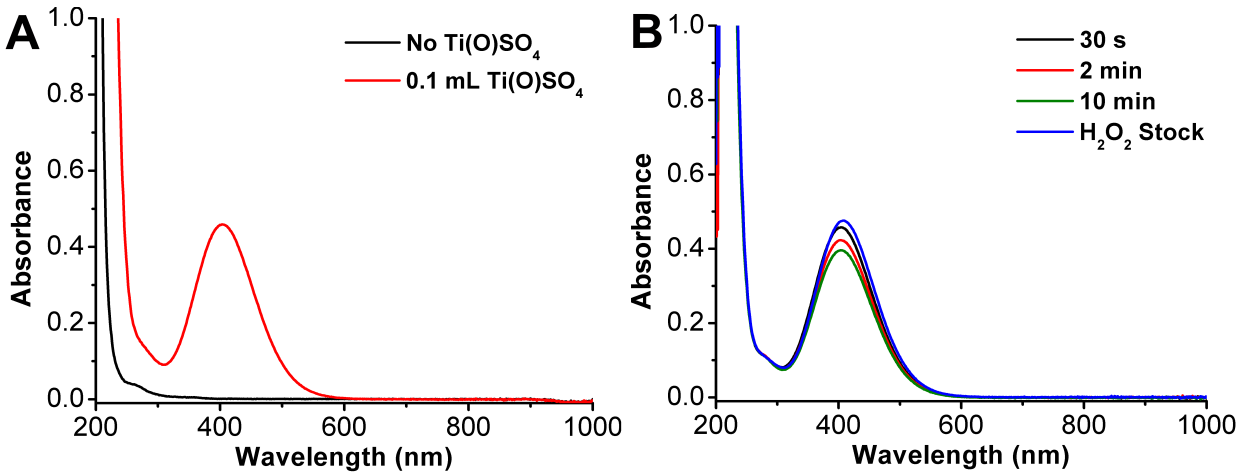

Figure S34. Stability test of urea•H_2O_2 in the presence of Mn($^{p\text{-}tbu}$dhbpy)Cl **1**, DIPEAHPF$_6$, DIPEA, and FeCp*$_2$ (A) before (black trace) and after (red trace) the addition of 0.1 mL of 0.1 M Ti(O)SO$_4$ to an extracted aliquot after 30 s. (B) Corrected UV-vis spectra (red – black from A) after 30 s (black), 120 s (red), 600 s (green), and H_2O_2 only (blue). Conditions: 40 µM Mn($^{p\text{-}tbu}$dhbpy)Cl, 10 mM DIPEAHPF$_6$/DIPEA, 2.3 mM urea•H_2O_2, 1 mM FeCp*$_2$ in MeCN.

Table S12. Summary of H_2O_2RR by Mn($^{p\text{-}tbu}$dhbpy)Cl **1** with 10 mM DIPEAHPF$_6$/DIPEA and 1 mM FeCp*$_2$ (**Figure S34**) relative to 2.3 mM H_2O_2 stock solution.

Time (s)	% H_2O_2 Recovered
30	94.1 ± 2.3
120	88.3 ± 1.9
540	82.9 ± 2.2

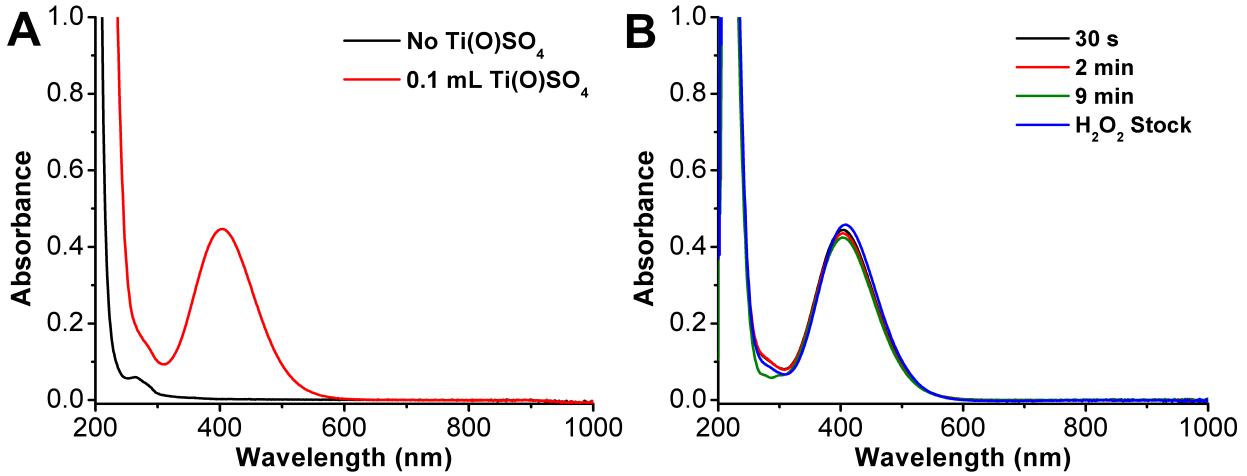

Figure S35. Stability test of urea•H_2O_2 in the presence of Mn(^{nPr}dhbpy)Cl **2**, DIPEAHPF$_6$, DIPEA, and FeCp*$_2$ (A) before (black trace) and after (red trace) the addition of 0.1 mL of 0.1 M Ti(O)SO$_4$ to an extracted aliquot after 30 s. (B) Corrected UV-vis spectra (red – black from A) after 30 s (black), 120 s (red), 600 s (green), and H_2O_2 only (blue). Conditions: 40 µM Mn(^{nPr}dhbpy)Cl, 10 mM DIPEAHPF$_6$/DIPEA, 2.3 mM urea•H_2O_2, 1 mM FeCp*$_2$ in MeCN.

Table S13. Summary of H_2O_2RR by Mn(^{nPr}dhbpy)Cl **2** with 10 mM DIPEAHPF$_6$/DIPEA and 1 mM FeCp*$_2$ (Figure S35) relative to 2.3 mM H_2O_2 stock solution.

Time (s)	% H_2O_2 Recovered
30	88.5 ± 1.2
120	91.1 ± 3.6
540	86.5 ± 4.5

Stopped-Flow Spectrochemical Methods. Stopped-flow spectrochemical kinetics studies were performed with a CSF-61DX2 Stopped-Flow System from Hi-Tech Scientific. Kinetic Studio Software was used to monitor a single wavelength and Integrated CCD Software was used to monitor the entire visible spectrum. All data fits were performed within the Kinetic Studio 4.0 Software Suite. Prior to experiments, dried and degassed MeCN was passed through syringes and the cell block before reagents were loaded. In a typical experiment, syringes would be charged with known concentrations of reagent. All reagent solutions were prepared immediately before use.

In general, a vial containing Mn catalyst and proton source (and conjugate base, if present) was sparged with O_2, drawn into a syringe and loaded into the stopped-flow. A second syringe containing N_2-saturated Cp*$_2$Fe solution loaded into the stopped-flow. All reported concentrations are the mixed concentrations in the spectroscopic cell.

Determination of the Rate Law for ORR by 1 under Unbuffered Conditions

$$\text{rate} = k_{cat}[Mn^{p-tbu}]^1[O_2]^1 \qquad \textbf{Eq S11}$$

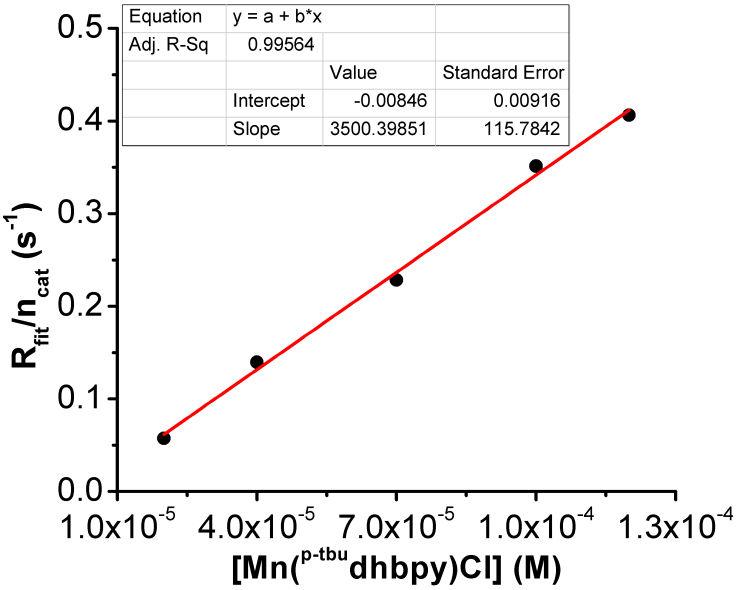

Figure S36. The calculated R_{fit}/n_{cat} values from stopped-flow spectrochemical experiments with DIPEAHPF$_6$, O_2, and Cp*$_2$Fe with varying Mn($^{p\text{-}tbu}$dhbpy)Cl **1** concentration. Data were fit using Kinetic Studio 4.0 (1Exp+Mx+C), n_{cat} = 2.72. Concentrations: DIPEAHPF$_6$ = 10 mM, O_2 = 4.05 mM, Cp*$_2$Fe = 1 mM.

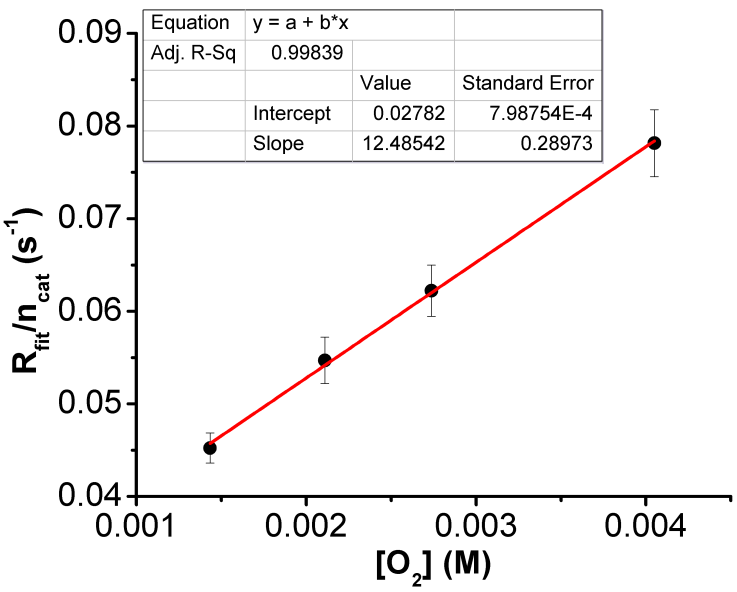

Figure S37. The calculated R_{fit}/n_{cat} values from stopped-flow spectrochemical experiments with Mn($^{p\text{-}tbu}$dhbpy)Cl **1**, DIPEAHPF$_6$, and Cp*$_2$Fe with varying O_2 concentration. Data were fit using Kinetic Studio 4.0 (1Exp+Mx+C), n_{cat} = 2.72. Concentrations: Mn($^{p\text{-}tbu}$dhbpy)Cl = 40 μM, DIPEAHPF$_6$ = 10 mM, Cp*$_2$Fe = 1 mM.

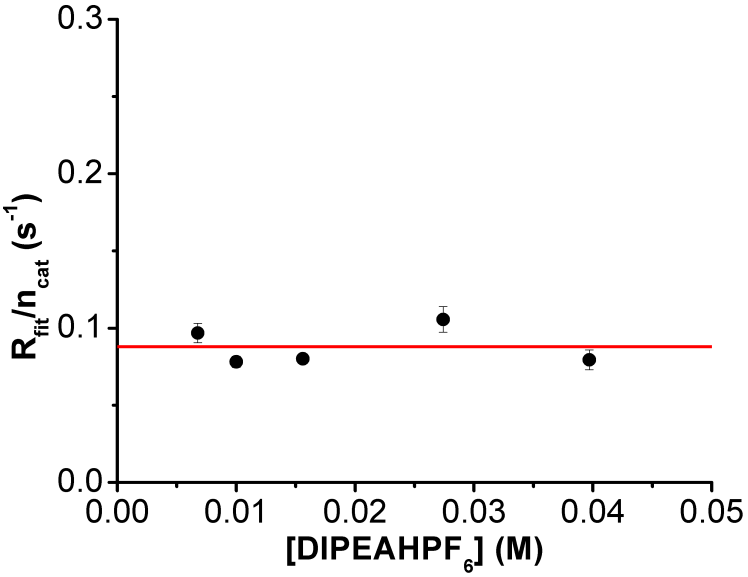

Figure S38. The calculated R_{fit}/n_{cat} values from stopped-flow spectrochemical experiments with Mn($^{p\text{-}tbu}$dhbpy)Cl **1**, O_2, and Cp*$_2$Fe with varying DIPEAHPF6 concentration. Data were fit using Kinetic Studio 4.0 (1Exp+Mx+C), n_{cat} = 2.72. The red line represents the global average over all points. Concentrations: Mn($^{p\text{-}tbu}$dhbpy)Cl = 40 μM, O_2 = 4.05 mM, Cp*$_2$Fe = 1 mM.

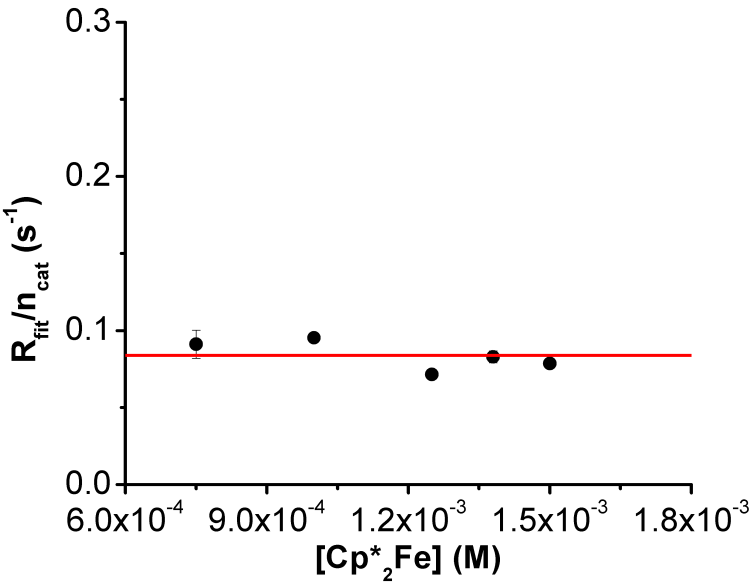

Figure S39. The calculated R_{fit}/n_{cat} values from stopped-flow spectrochemical experiments with Mn($^{p\text{-}tbu}$dhbpy)Cl **1**, O_2, and DIPEAHPF$_6$ with varying Cp*$_2$Fe concentration. Data were fit using Kinetic Studio 4.0 (1Exp+Mx+C), n_{cat} = 2.72. The red line represents the global average over all points. Concentrations: Mn($^{p\text{-}tbu}$dhbpy)Cl = 40 μM, O_2 = 4.05 mM, DIPEAHPF$_6$ = 10 mM.

Determination of the Rate Law of ORR by 1 under Buffered Conditions

$$rate = k_{cat}[Mn^{p-tbu}]^1[O_2]^1 \qquad \textbf{Eq S12}$$

Comparable k_{obs} values can be obtained from the average of R_{fit}/n_{cat} values across independent experimental data points at identical conditions: 40 μM [Mn], 10 mM [DIPEAHPF$_6$/DIPEA], 4.05 mM [O_2], and 1 mM [Cp*$_2$Fe] (**Figures S40–S44**).

$$k_{obs} = 1.23 \pm 0.17 \times 10^{-1}\ s^{-1}$$

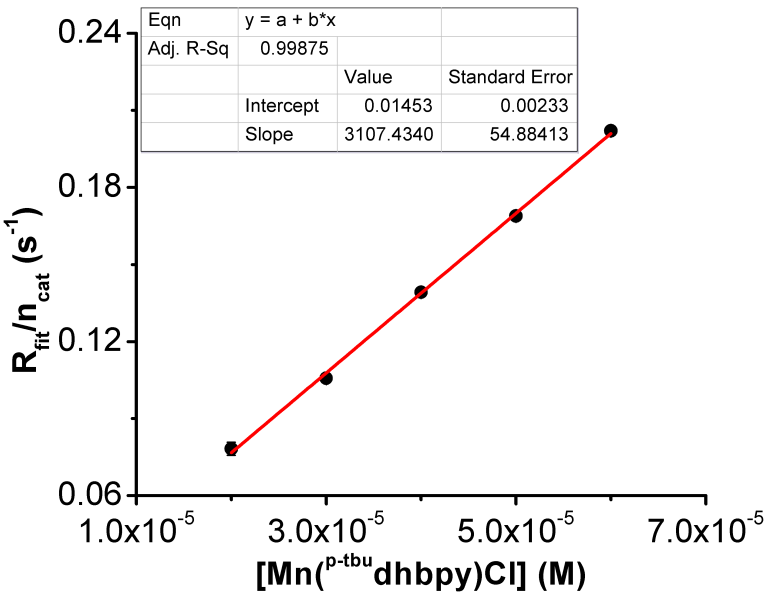

Figure S40. The calculated R_{fit}/n_{cat} values from stopped-flow spectrochemical experiments with DIPEAHPF$_6$, DIPEA, O_2, and Cp*$_2$Fe with varying Mn($^{p\text{-}tbu}$dhbpy)Cl **1** concentration. Data were fit using Kinetic Studio 4.0 (1Exp+Mx+C), n_{cat} = 3.64. Concentrations: DIPEAHPF$_6$/DIPEA = 10 mM, O_2 = 4.05 mM, Cp*$_2$Fe = 1 mM.

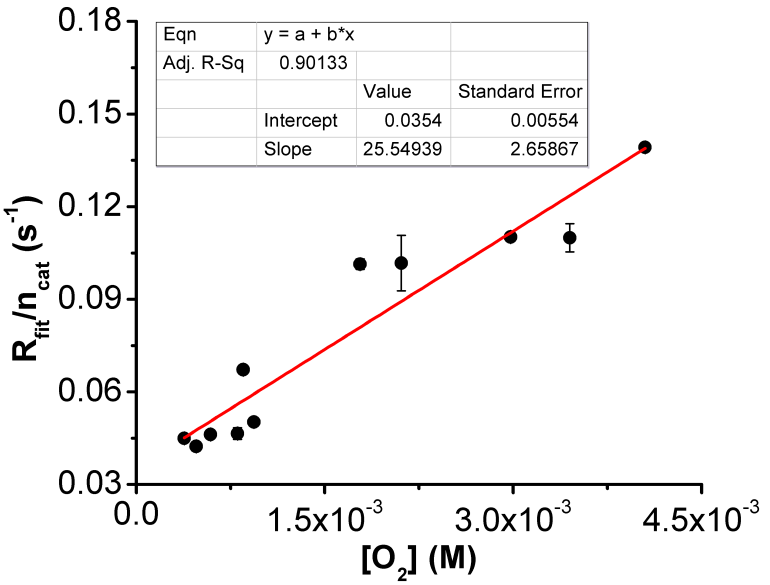

Figure S41. The calculated R_{fit}/n_{cat} values from stopped-flow spectrochemical experiments with Mn($^{p\text{-}tbu}$dhbpy)Cl **1**, DIPEAHPF$_6$, DIPEA, and Cp*$_2$Fe with varying O_2 concentration. Data were fit using Kinetic Studio 4.0 (1Exp+Mx+C), n_{cat} = 3.64. Concentrations: Mn($^{p\text{-}tbu}$dhbpy)Cl = 40 μM, DIPEAHPF$_6$/DIPEA = 10 mM, Cp*$_2$Fe = 1 mM.

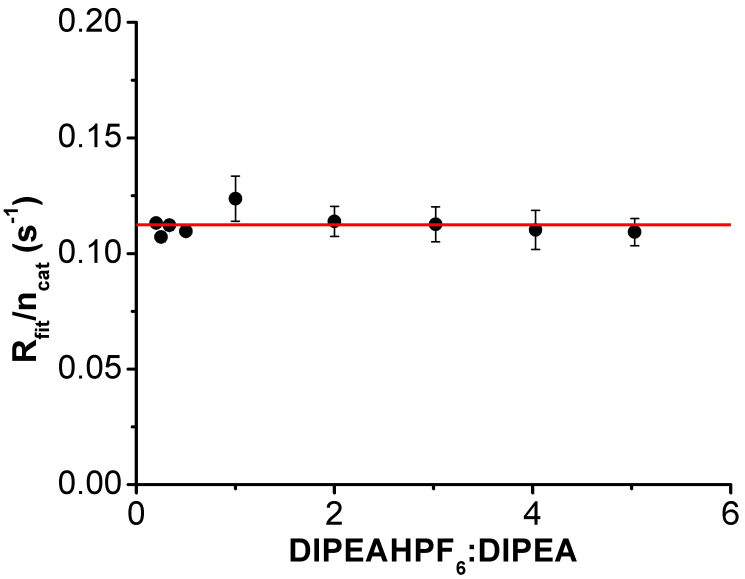

Figure S42. The calculated R_{fit}/n_{cat} values from stopped-flow spectrochemical experiments with Mn($^{p\text{-}tbu}$dhbpy)Cl **1**, O_2, DIPEA, and Cp*$_2$Fe with varying DIPEAHPF$_6$:DIPEA ratio. Data were fit using Kinetic Studio 4.0 (1Exp+Mx+C). The red line represents the global average over all points, n_{cat} = 3.64. Concentrations: Mn($^{p\text{-}tbu}$dhbpy)Cl = 40 μM, DIPEA = 10 mM, O_2 = 4.05 mM, Cp*$_2$Fe = 1 mM; 1:1 DIPEAHPF$_6$:DIPEA = 10 mM of each and all concentrations are relative to this point.

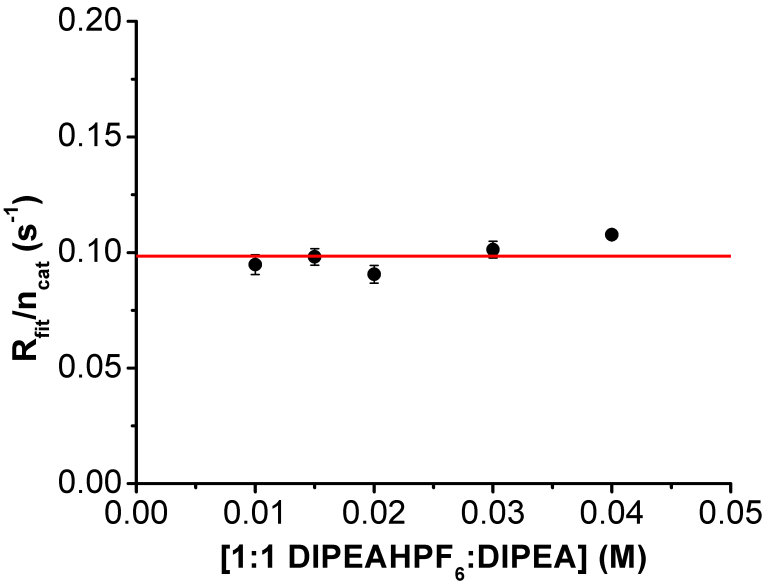

Figure S43. The calculated R_{fit}/n_{cat} values from stopped-flow spectrochemical experiments with Mn($^{p\text{-}tbu}$dhbpy)Cl **1**, O_2, and Cp*$_2$Fe with varying buffer (DIPEAHPF$_6$ and DIPEA, 1:1 ratio) concentration. Data were fit using Kinetic Studio 4.0 (1Exp+Mx+C). The red line represents the global average over all points, n_{cat} = 3.64. Concentrations: Mn($^{p\text{-}tbu}$dhbpy)Cl = 40 μM, O_2 = 4.05 mM, Cp*$_2$Fe = 1 mM.

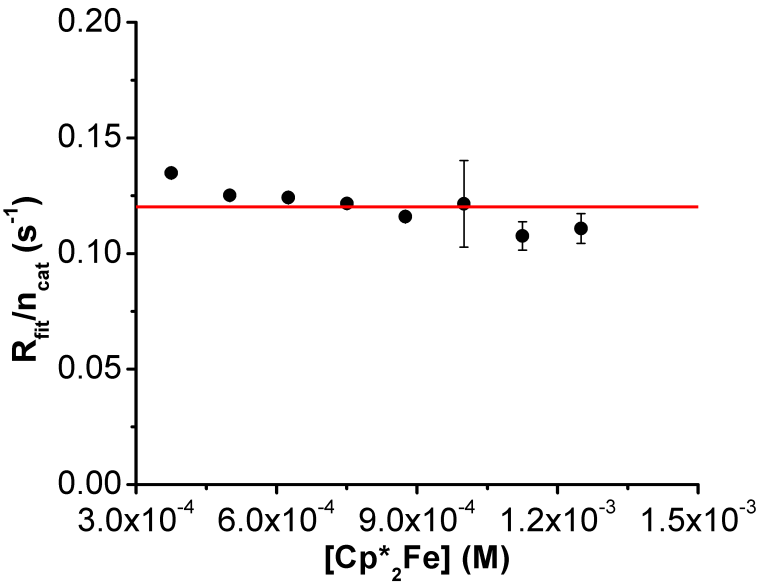

Figure S44. The calculated R_{fit}/n_{cat} values from stopped-flow spectrochemical experiments with Mn($^{p\text{-}tbu}$dhbpy)Cl **1**, DIPEAHPF$_6$, DIPEA, and O_2 with varying Cp*$_2$Fe concentration. Data were fit using Kinetic Studio 4.0 (1Exp+Mx+C). The red line represents the global average over all points, n_{cat} = 3.64. Concentrations: Mn($^{p\text{-}tbu}$dhbpy)Cl = 40 μM, O_2 = 4.05 mM, DIPEAHPF$_6$/DIPEA = 10 mM.

Determination of Rate Law of ORR by 2 under Unbuffered Conditions

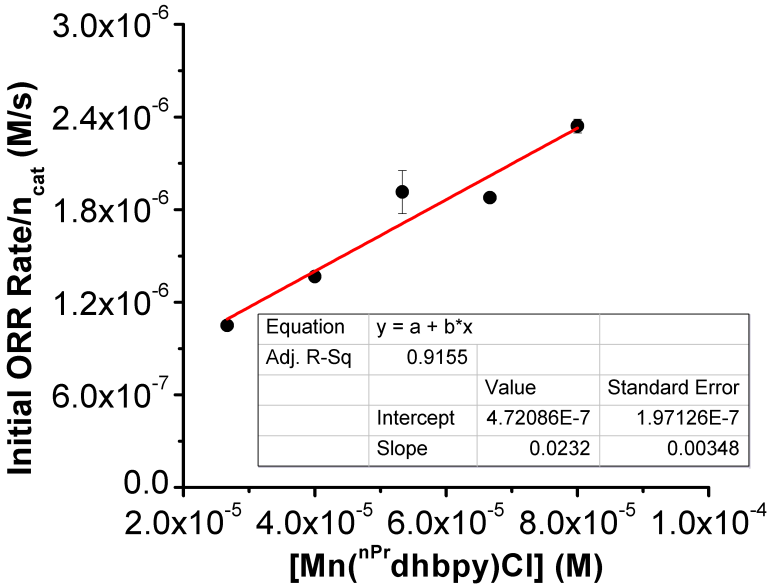

Figure S45. The calculated initial ORR rate from stopped-flow spectrochemical experiments with DIPEAHPF$_6$, O_2, Cp*$_2$Fe with varying Mn(^{nPr}dhbpy)Cl **2** concentration. Data were fit using Kinetic Studio 4.0 (Linear) correcting for the concentration of Cp*$_2$Fe and n_{cat} = 2.08 Concentrations: DIPEAHPF$_6$ = 10 mM, O_2 = 4.05 mM, and Cp*$_2$Fe = 1 mM.

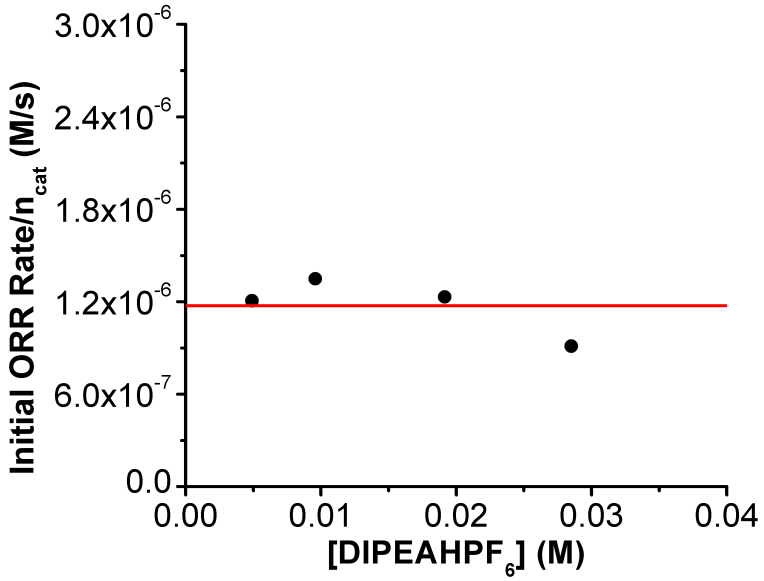

Figure S46. The calculated initial ORR rate from stopped-flow spectrochemical experiments with, Mn(^{nPr}dhbpy)Cl **2**, O_2, Cp^*_2Fe with varying DIPEAHPF$_6$ concentration. Data were fit using Kinetic Studio 4.0 (Linear) correcting for the concentration of Cp^*_2Fe and n_{cat} = 2.08. Concentrations: Mn(^{nPr}dhbpy)Cl = 40 μM, O_2 = 4.05 mM, and Cp^*_2Fe = 1 mM.

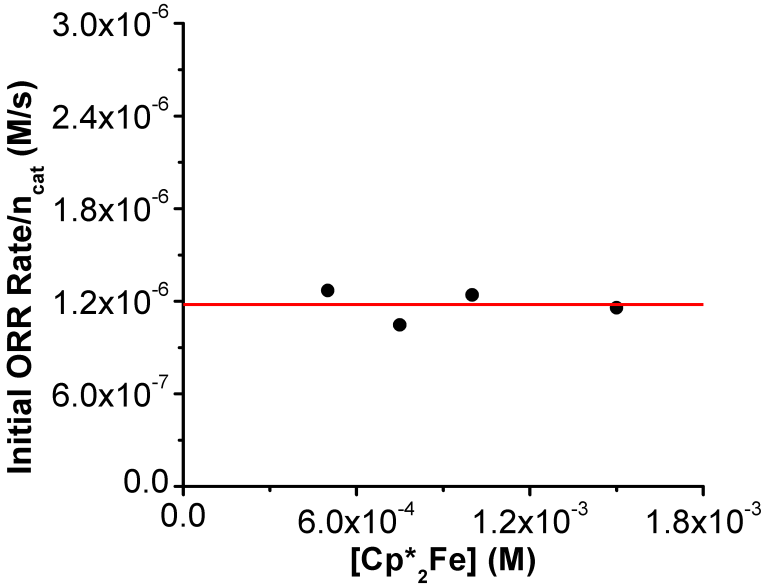

Figure S47. The calculated initial ORR rate from stopped-flow spectrochemical experiments with, Mn(^{nPr}dhbpy)Cl **2**, DIPEAHPF$_6$, O_2, with varying Cp^*_2Fe concentration. Data were fit using Kinetic Studio 4.0 (Linear) and correcting for the concentration of Cp^*_2Fe and n_{cat} = 2.08. Concentrations: Mn(^{nPr}dhbpy)Cl = 40 μM, O_2 = 4.05 mM, and DIPEAHPF$_6$ = 10 mM.

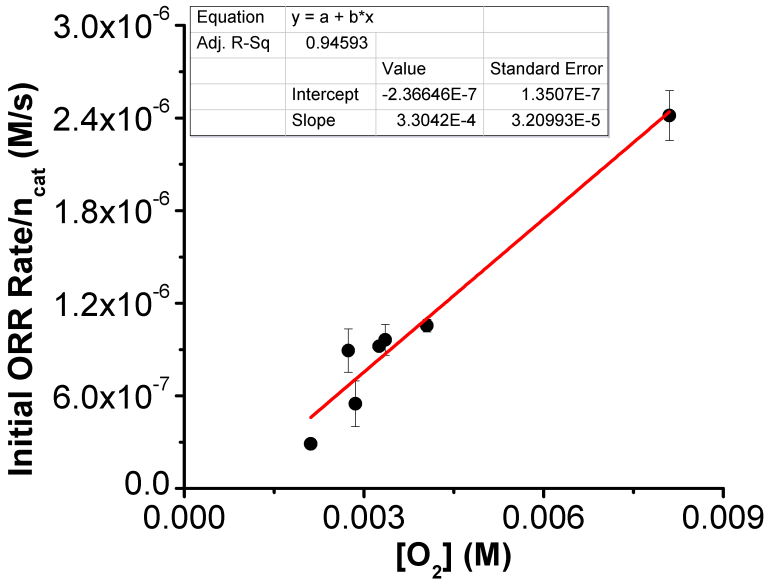

Figure S48. The calculated initial ORR rate from stopped-flow spectrochemical experiments with, Mn(^{nPr}dhbpy)Cl **2**, DIPEAHPF$_6$, Cp*$_2$Fe with varying O_2, concentration. Data were fit using Kinetic Studio 4.0 (Linear) and correcting for the concentration of Cp*$_2$Fe and n_{cat} = 2.08. Concentrations: Mn(^{nPr}dhbpy)Cl = 40 μM, O_2 = 4.05 mM, and DIPEAHPF$_6$ = 10 mM.

Determination of Rate Law for ORR by 2 under Buffered Conditions

$$rate = k_{cat}[Mn^{nPr}]^2[DIPEA]^1[Cp^*{}_2Fe]^{-1} \quad \textbf{Eq S13}$$

Comparable k_{obs} values can be obtained from the average of R_{fit}/n_{cat} values across independent experimental data points at identical conditions: 40 μM [Mn], 10 mM [DIPEAHPF$_6$/DIPEA], 4.05 mM [O_2], and 1 mM [Cp*$_2$Fe] (**Figures S49-S53**).

$$k_{obs} = 0.706 \pm 0.25 \times 10^{-1}\ s^{-1}$$

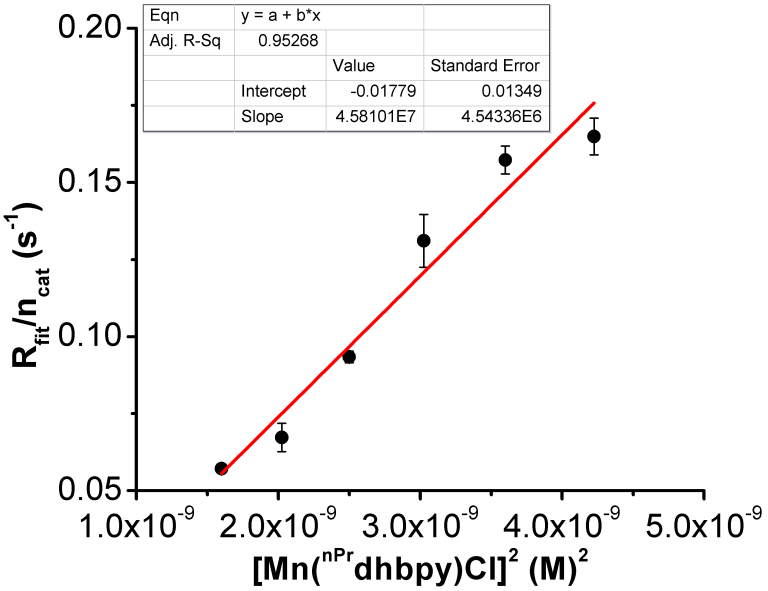

Figure S49. The calculated R_{fit}/n_{cat} values from stopped-flow spectrochemical experiments with DIPEAHPF$_6$, DIPEA, O_2, and Cp*$_2$Fe with varying Mn(^{nPr}dhbpy)Cl **2** concentration. Data were fit using Kinetic Studio 4.0 (1Exp+Mx+C), n_{cat} = 3.24. Concentrations: DIPEAHPF$_6$/DIPEA = 10 mM, O_2 = 4.05 mM, Cp*$_2$Fe = 1 mM.

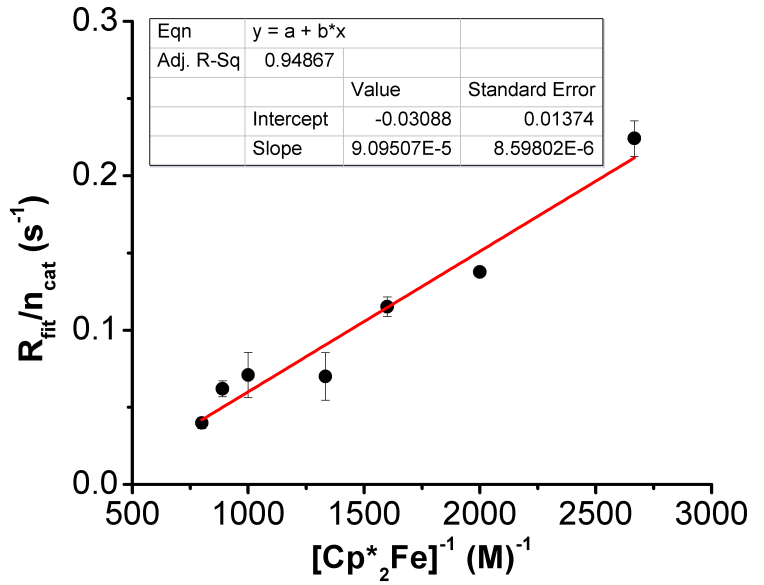

Figure S50. The calculated R_{fit}/n_{cat} values from stopped-flow spectrochemical experiments with Mn(^{nPr}dhbpy)Cl **2**, DIPEAHPF$_6$, DIPEA, and O_2 with varying Cp*$_2$Fe concentration. Data were fit using Kinetic Studio 4.0 (1Exp+Mx+C); n_{cat} = 3.24. Concentrations: Mn(^{nPr}dhbpy)Cl = 40 μM, O_2 = 4.05 mM, DIPEAHPF$_6$/DIPEA = 10 mM.

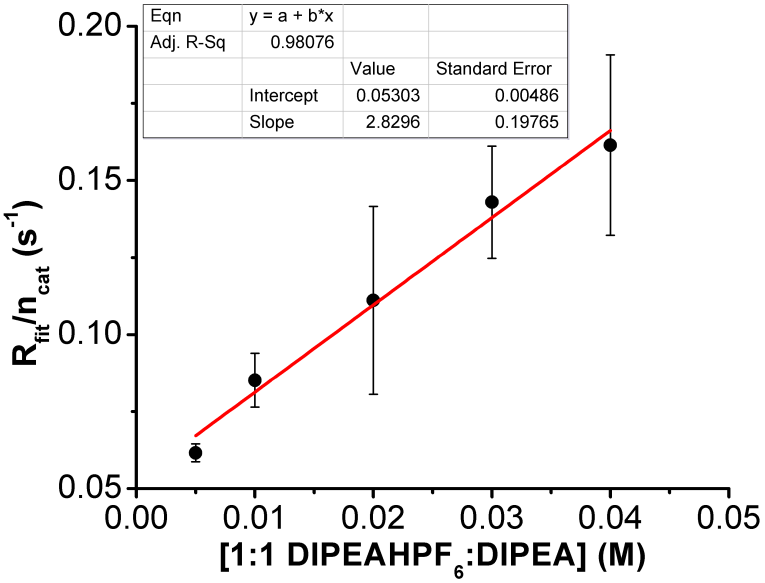

Figure S51. The calculated R_{fit}/n_{cat} values from stopped-flow spectrochemical experiments with Mn(^{nPr}dhbpy)Cl **2**, O_2, and Cp*$_2$Fe with varying buffer (DIPEAHPF$_6$ and DIPEA, 1:1 ratio) concentration. Data were fit using Kinetic Studio 4.0 (1Exp+Mx+C); n_{cat} = 3.24. Concentrations: Mn(^{nPr}dhbpy)Cl = 40 μM, O_2 = 4.05 mM, Cp*$_2$Fe = 1 mM.

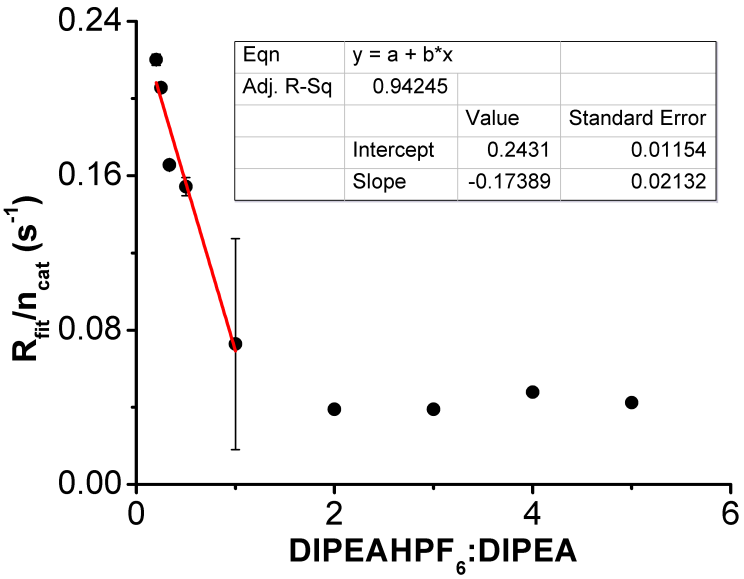

Figure S52. The calculated R_{fit}/n_{cat} values from stopped-flow spectrochemical experiments with Mn(^{nPr}dhbpy)Cl **2**, O_2, and Cp*$_2$Fe with varying DIPEAHPF$_6$:DIPEA ratio. Data were fit using Kinetic Studio 4.0 (1Exp+Mx+C); n_{cat} = 3.24. Concentrations: Mn($^{p\text{-}tbu}$dhbpy)Cl = 40 μM, O_2 = 4.05 mM, 1:1 DIPEAHPF$_6$:DIPEA = 10 mM, Cp*$_2$Fe = 1 mM; 1:1 DIPEAHPF$_6$:DIPEA = 10 mM and all concentrations are relative to this point.

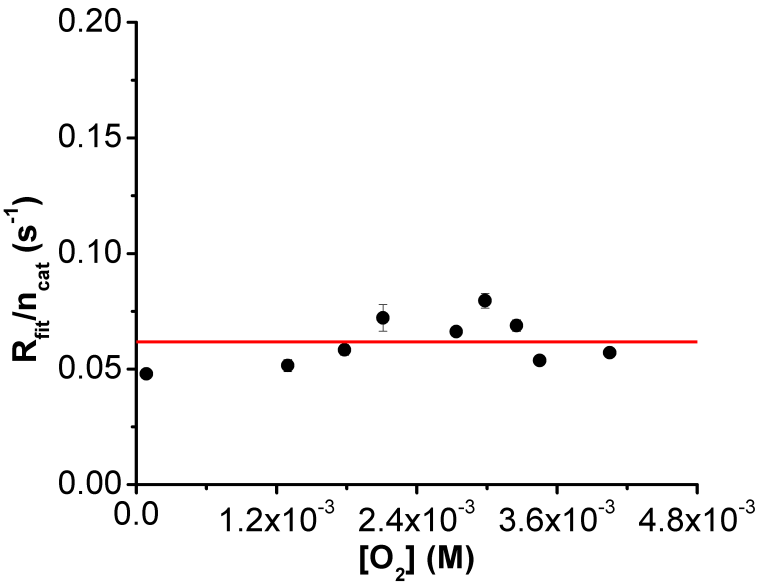

Figure S53. The calculated R_{fit}/n_{cat} values from stopped-flow spectrochemical experiments with Mn(^{nPr}dhbpy)Cl **2**, DIPEAHPF$_6$, DIPEA, and Cp*$_2$Fe with varying O_2 concentration. Data were fit using Kinetic Studio 4.0 (1Exp+Mx+C); n_{cat} = 3.24. Concentrations: Mn(^{nPr}dhbpy)Cl = 40 μM, DIPEAHPF$_6$ = 10 mM, DIPEA = 10 mM, Cp*$_2$Fe = 1 mM.

Description of Stopped-Flow Data Fitting

1Exp+Mx+C Fits

For the rate law determination of ORR by Mn($^{p\text{-}tbu}$dhbpy)Cl **1** with and without the presence of DIEPA and by Mn(^{nPr}dhbpy)Cl **2** with the presence of DIPEA, Kinetic Studio 4.0 was used to fit data sets with 1Exp+Mx+C. R_{fit} values were obtained by fitting the increase in absorbance at 780 nm versus time to a single exponential (1Exp+Mx+C) to achieve an R^2 value of 0.99 (See Figures S54-S56). Where the fit equation contains an exponent (1Exp), a linear portion (Mx) and a non-zero intercept (C). The R_{fit} values were corrected for the number of electrons passed during catalysis and plotted against variable concentrations to obtain the experimental rate law.

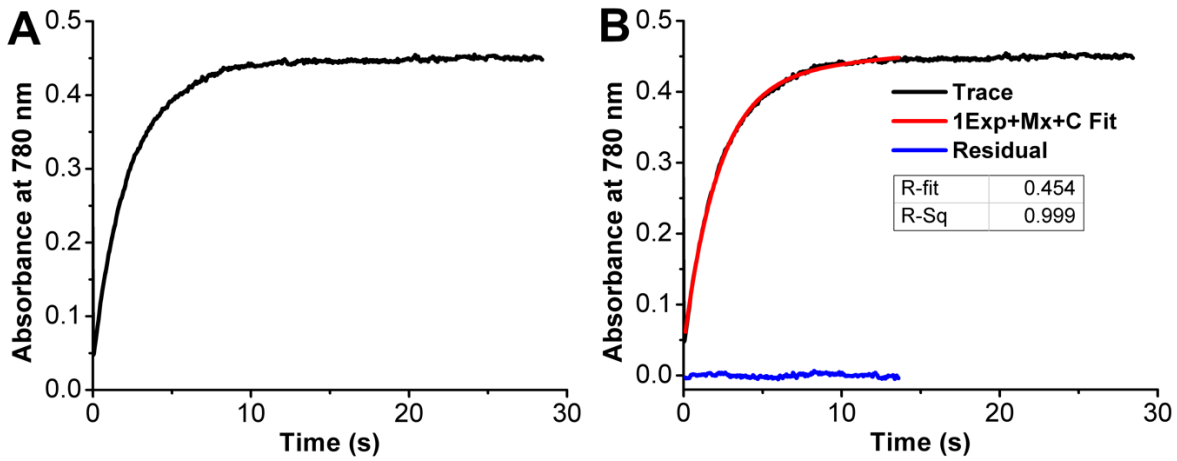

Figure S54. (A) Representative trace of time versus absorbance at 780 nm for ORR catalyzed by Mn($^{p\text{-}tbu}$dhbpy)Cl **1** with DIPEAHPF$_6$/DIPEA and (B) the 1Exp+Mx+C fit (red) and residual (blue) used for data analysis using the Kinetic Studio 4.0 software. Conditions: Mn($^{p\text{-}tbu}$dhbpy)Cl = 40 μM, Cp*$_2$Fe = 1 mM, O_2 = 4.05 mM, and DIPEAHPF$_6$/DIEPA = 10 mM.

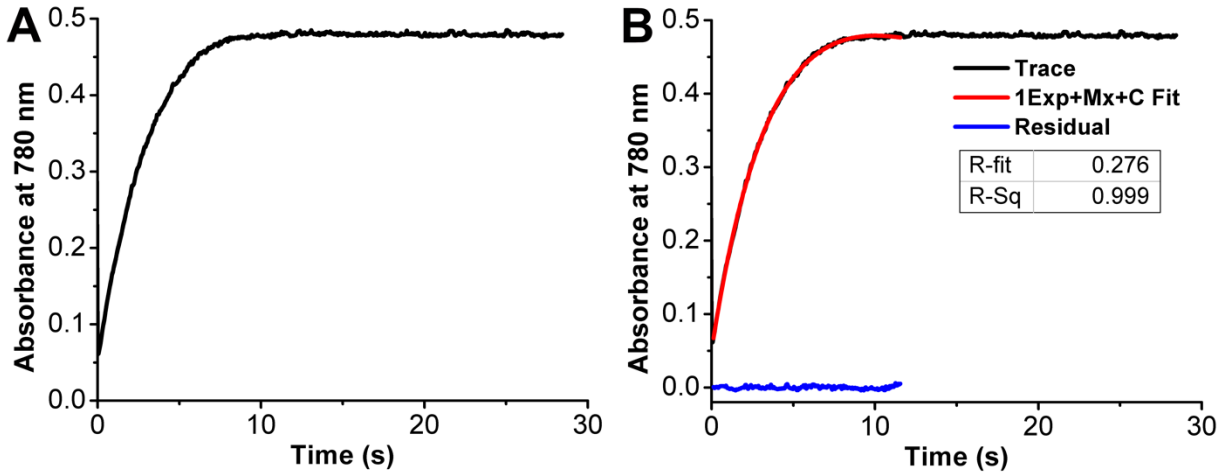

Figure S55. (A) Representative trace of time versus absorbance at 780 nm for ORR catalyzed by Mn(^{nPr}dhbpy)Cl **2** with DIPEAHPF$_6$/DIPEA and (B) the 1Exp+Mx+C fit (red) and residual (blue) used for data analysis using the Kinetic Studio 4.0 software. Conditions: Mn(^{nPr}dhbpy)Cl = 40 μM, Cp*$_2$Fe = 1 mM, O_2 = 4.05 mM, and DIPEAHPF$_6$/DIEPA = 10 mM.

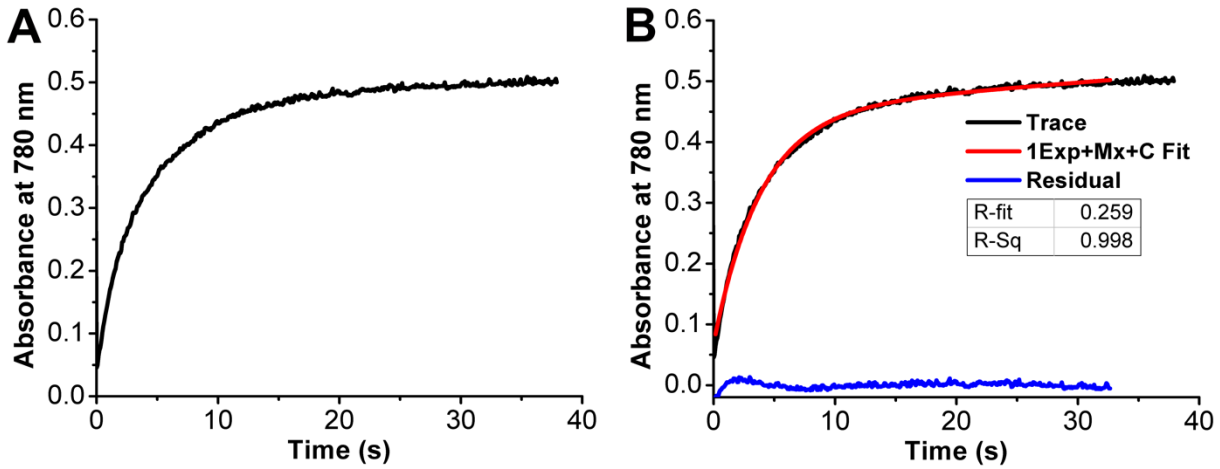

Figure S56. (A) Representative trace of time versus absorbance at 780 nm for ORR catalyzed by Mn($^{p\text{-}tbu}$dhbpy)Cl **1** with DIPEAHPF$_6$ and (B) the 1Exp+Mx+C fit (red) and residual (blue) used for data analysis using the Kinetic Studio 4.0 software. Conditions: Mn($^{p\text{-}tbu}$dhbpy)Cl = 40 μM, Cp*$_2$Fe = 1 mM, O_2 = 4.05 mM, and DIPEAHPF$_6$ = 10 mM.

Initial Rates Method

For the rate law determination of ORR by Mn(^{nPr}dhbpy)Cl **2** without the presence of DIPEA, the initial rates method was used due to the linearity of the observed curve. In this case, Initial ORR Rate values were obtained by taking slope of the linear fit of the initial region (~1.5 to ~50 s) in the Kinetic Studio 4.0 software of [Cp*$_2$Fe]$^+$ growth at 780 nm (units = relative absorbance/second). The results of the linear fit were processed to reflect the rate of ORR by converting the relative absorbance units to concentration using the molar extinction coefficient of [Cp*$_2$Fe]$^+$ (ε = 461 $M^{-1}cm^{-1}$ as determined by serial dilution of a chemical prepared sample of [Cp*$_2$Fe][BF$_4$]) and correcting for the number of electrons passed during catalysis (n_{cat} = 2.08). See **Figure S57** for description of the linear fits.

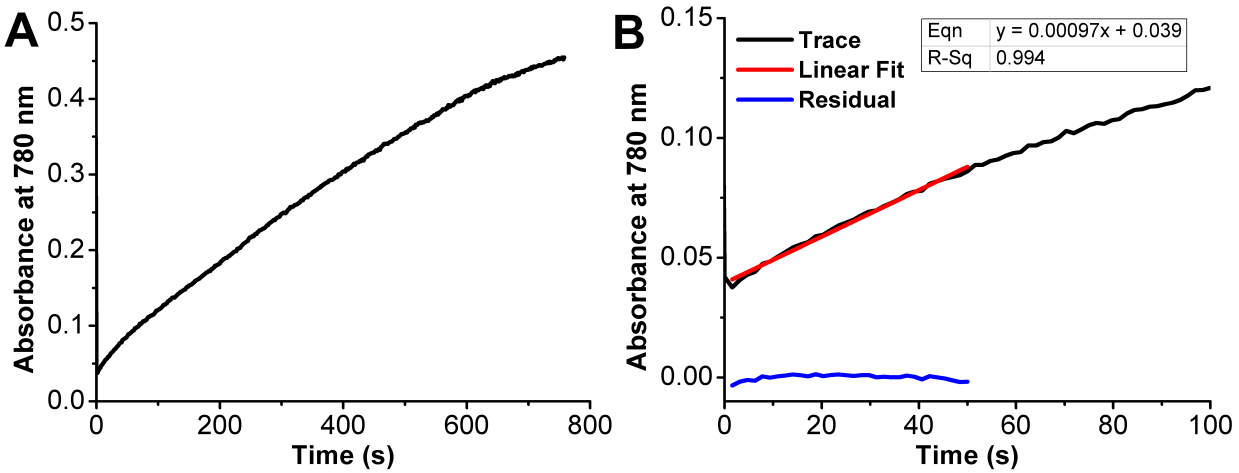

Figure S57. (A) Representative trace of time versus absorbance at 780 nm for ORR catalyzed by Mn(^{nPr}dhbpy)Cl **2** with DIPEAHPF$_6$ and (B) the initial Linear fit (red) and residual (blue) used for data analysis using the Kinetic Studio 4.0 software. Conditions: Mn(^{nPr}dhbpy)Cl = 40 μM, Cp*$_2$Fe = 1 mM, O_2 = 4.05 mM, and DIPEAHPF$_6$ = 10 mM.

UV-vis Spectroscopic Analysis

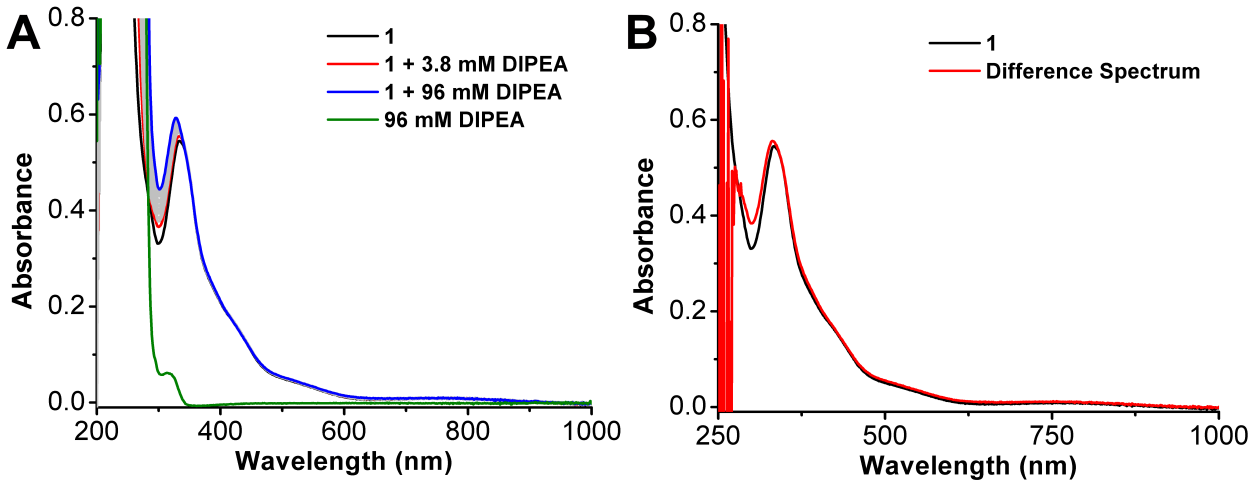

Figure S58. (A) UV-vis of spectra of 23 μM Mn($^{p\text{-}tbu}$dhbpy)Cl **1** with increasing amounts of DIPEA in MeCN (B) difference spectrum of the final titration point (blue – green traces). Conditions: quartz cuvette with 1 cm pathlength; [DIPEA] = 3.8, 7.7, 12, 15.3, 19, 29, 38, 48, 57, 67, 77, 86, 96 mM.

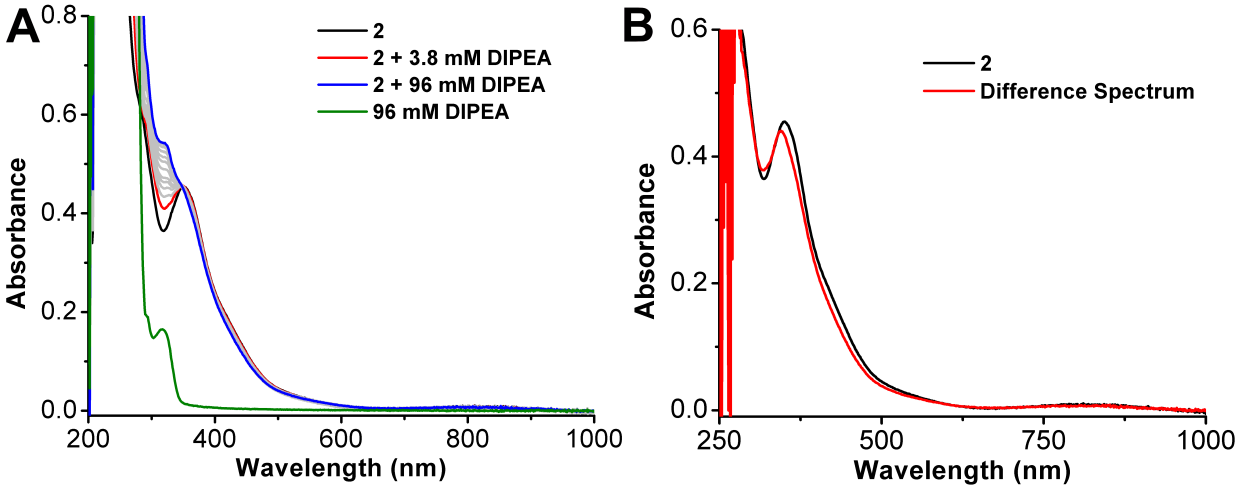

Figure S59. (A) UV-vis of spectra of 26.8 μM Mn(^{nPr}dhbpy)Cl **2** with increasing amounts of DIPEA in MeCN (B) difference spectrum of the final titration point (blue – green traces). Conditions: quartz cuvette with 1 cm pathlength; [DIPEA] = 3.8, 7.7, 12, 15.3, 19, 29, 38, 48, 57, 67, 77, 86, 96 mM.

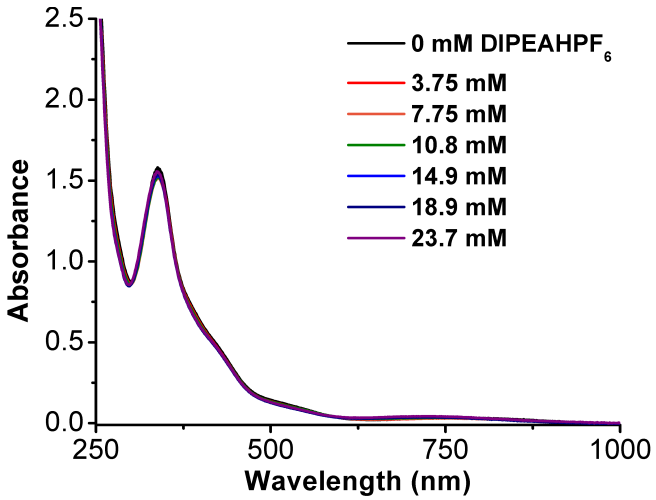

Figure S60. UV-vis of spectra of 80 μM Mn($^{p\text{-}tbu}$dhbpy)Cl **1** with increasing amounts of $DIPEAHPF_6$. Conditions: quartz cuvette with 1 cm pathlength.

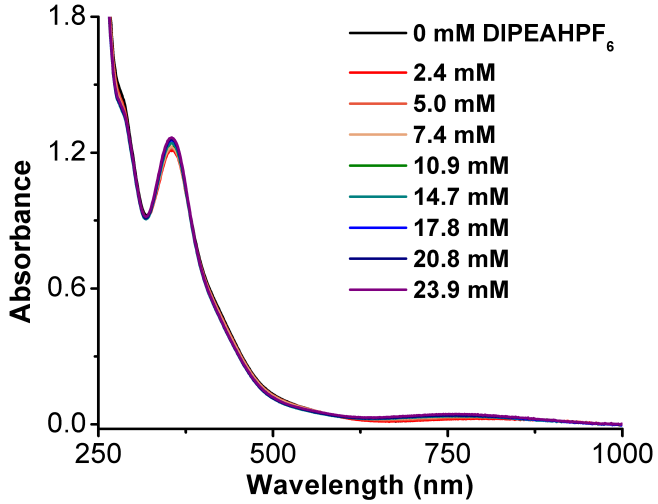

Figure S61. (A) UV-vis spectra of 80 μM Mn(^{nPr}dhbpy)Cl **2** with increasing amounts of $DIPEAHPF_6$ in MeCN. Conditions: quartz cuvette with 1 cm pathlength.

UV-vis Spectroscopic Studies of Mn($^{p\text{-}tbu}$dhbpy)Cl 1 and Cobaltocene

In order to better understand the reactivity of reduced Mn($^{p\text{-}tbu}$dhbpy)Cl **1** and Mn(^{nPr}dhbpy)Cl **2**, we used cobaltocene ($CoCp_2$) as a chemical reductant in solution. Solutions were prepared in a N_2 filled glovebox. To expose solutions to O_2, the cuvette was opened and inverted.

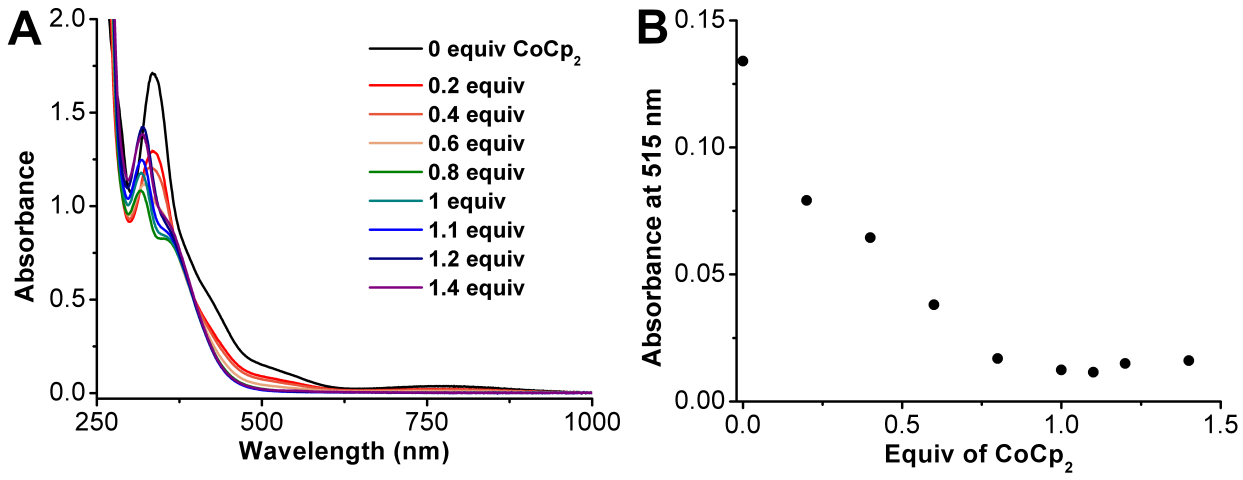

Figure S62. (A) UV-vis spectra of an 80 μM solution of Mn($^{p\text{-}tbu}$dhbpy)Cl **1** with increasing amounts of $CoCp_2$ in MeCN under N_2. (B) Absorbance at 515 nm versus equivalents of $CoCp_2$ relative to [**1**]. Conditions: quartz cuvette with 1 cm pathlength.

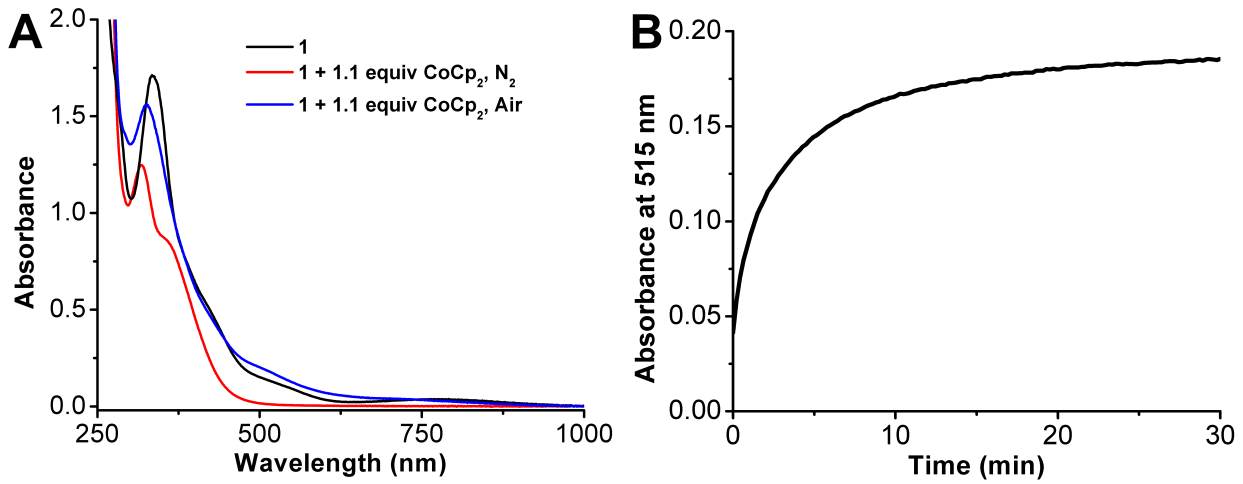

Figure S63. (A) UV-vis spectra of 80 μM solution of Mn($^{p\text{-}tbu}$dhbpy)Cl **1** in MeCN (black) under N_2 with 1.1 equiv of $CoCp_2$ (red) and after being exposed to air for 30 min (blue). (B) Time versus absorbance at 515 nm upon exposure of a 80 μM solution of Mn($^{p\text{-}tbu}$dhbpy)Cl with 1.1 equiv $CoCp_2$ to air. Conditions: quartz cuvette with 1 cm pathlength.

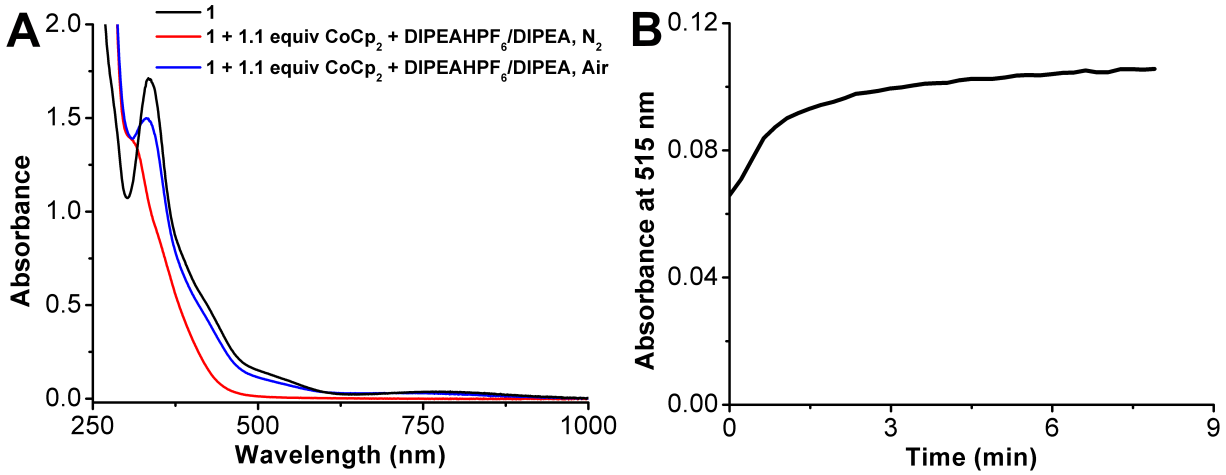

Figure S64. (A) UV-vis spectra of 80 μM solution of Mn($^{p\text{-}tbu}$dhbpy)Cl **1** in MeCN (black) under N_2 with 1.1 equiv of $CoCp_2$ and 19.7 mM DIPEAHPF6/DIPEA (red) and after being exposed to air for 8 min (blue). (B) Time versus absorbance at 515 nm upon exposure of a 80 μM solution of Mn($^{p\text{-}tbu}$dhbpy)Cl with 1.1 equiv $CoCp_2$ and 19 mM $DIPEAHPF_6$/DIPEA to air. Conditions: quartz cuvette with 1 cm pathlength.

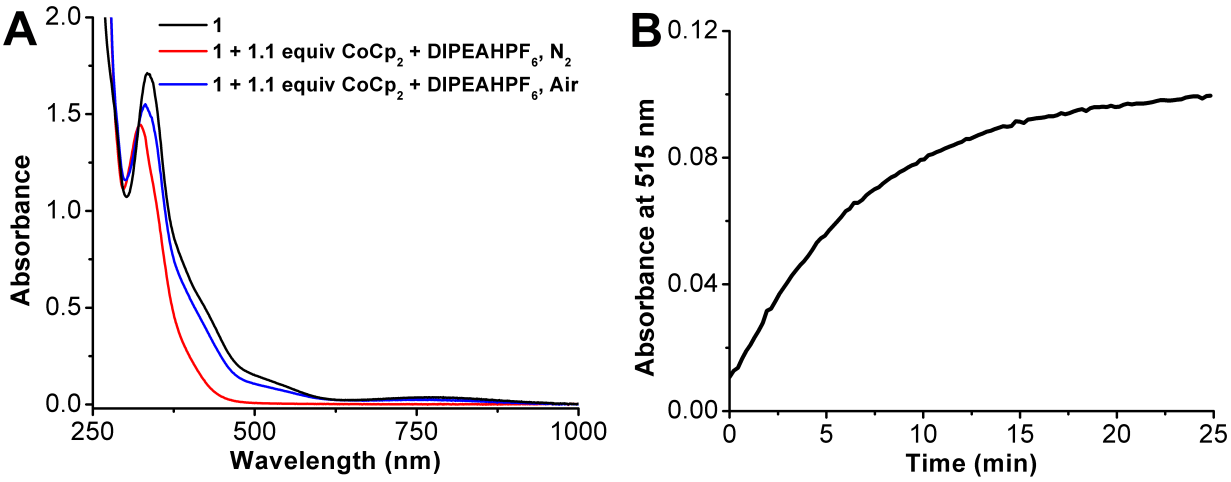

Figure S65. (A) UV-vis spectra of 80 μM solution of Mn($^{p\text{-}tbu}$dhbpy)Cl **1** in MeCN (black) under N_2 with 1.1 equiv of $CoCp_2$ and 19.7 mM $DIPEAHPF_6$ (red) and after being exposed to air for 25 min (blue). (B) Time versus absorbance at 515 nm upon exposure of a 80 μM solution of Mn($^{p\text{-}tbu}$dhbpy)Cl with 1.1 equiv $CoCp_2$ and 19.7 mM $DIPEAHPF_6$ to air. Conditions: quartz cuvette with 1 cm pathlength.

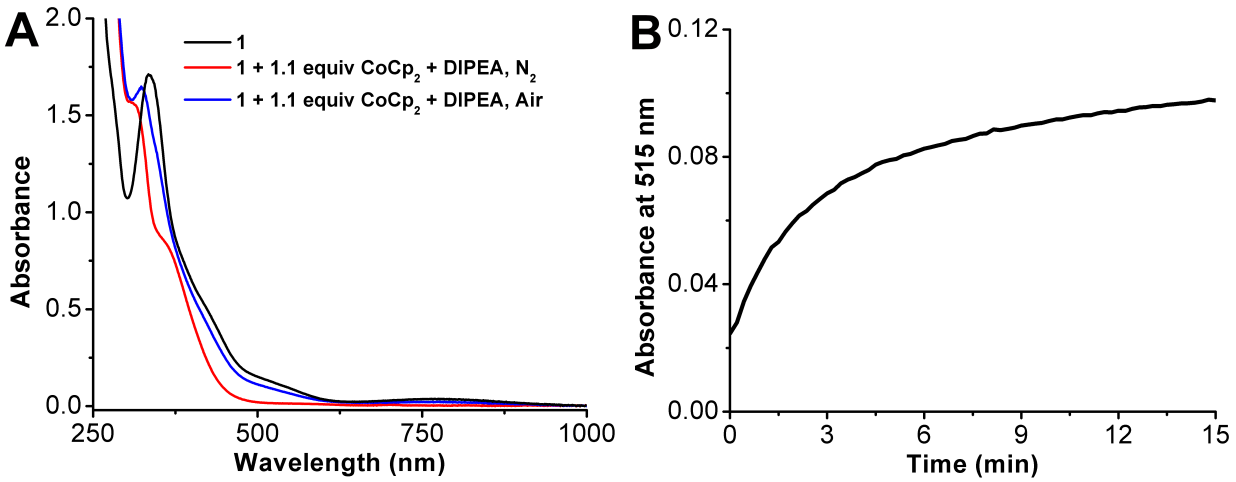

Figure S66. (A) UV-vis spectra of 80 μM solution of Mn($^{p\text{-tbu}}$dhbpy)Cl **1** in MeCN (black) under N_2 with 1.1 equiv of $CoCp_2$ and 19 mM DIPEA (red) and after being exposed to air for 15 min (blue). (B) Time versus absorbance at 515 nm upon exposure of a 80 μM solution of Mn($^{p\text{-tbu}}$dhbpy)Cl with 1.1 equiv $CoCp_2$ and 19 mM DIPEA to air. Conditions: quartz cuvette with 1 cm pathlength.

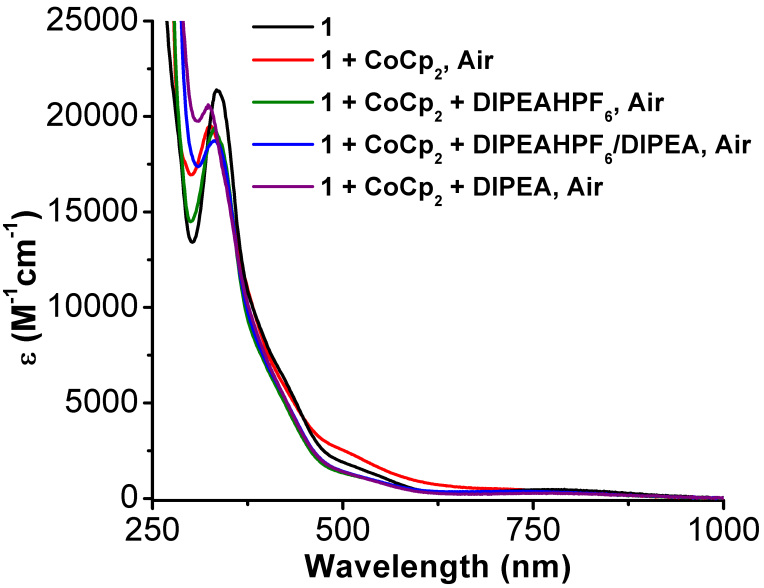

Figure S67. Overlay of data involving Mn($^{p\text{-tbu}}$dhbpy)Cl **1** from **Figs S63-S66** after samples were allowed to react with air completely.

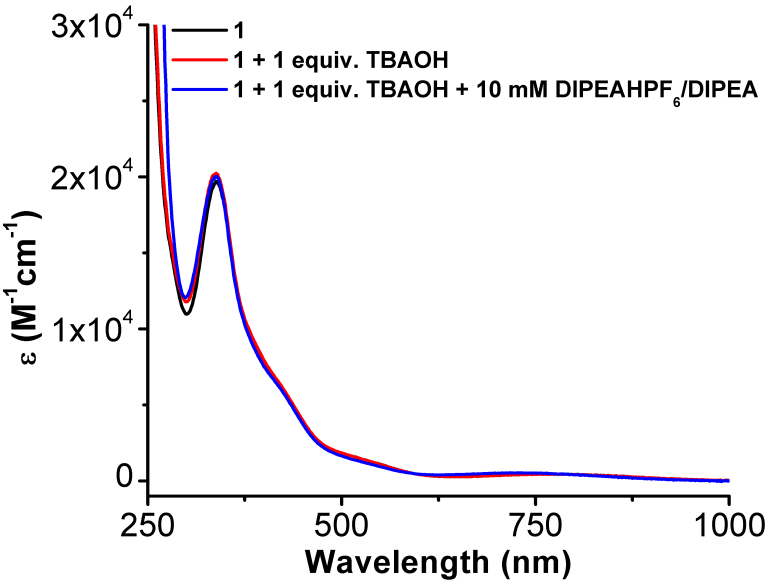

Figure S68. UV-vis spectra of 80 μM Mn($^{p\text{-}tbu}$dhbpy)Cl **1** with (red) and without (black) 1 equiv TBAOH•30H_2O and with of 10 mM buffer (1:1 DIPEAHPF_6:DIPEA) in the presence of 1 equiv TBAOH•30H_2O (blue). Conditions: quartz cuvette with 1 cm pathlength.

UV-vis Spectroscopic Studies of Mn(^{nPr}dhbpy)Cl 2 and Cobaltocene

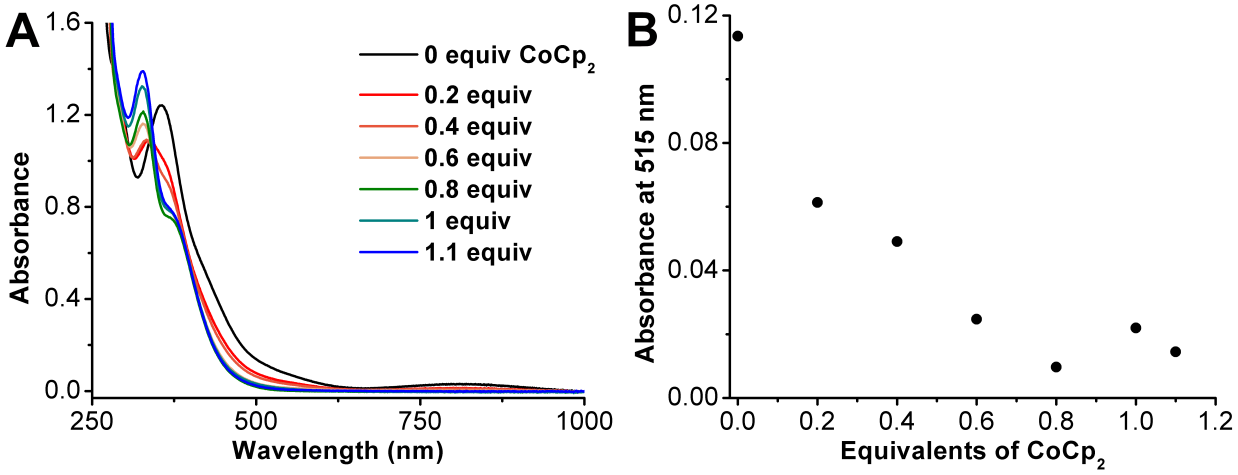

Figure S69. (A) UV-vis spectra of an 80 μM solution of Mn(^{nPr}dhbpy) **2** with increasing amounts of $CoCp_2$ in MeCN under N_2. (B) Absorbance at 515 nm versus equivalents of $CoCp_2$ relative to [**2**]. Conditions: quartz cuvette with 1 cm pathlength.

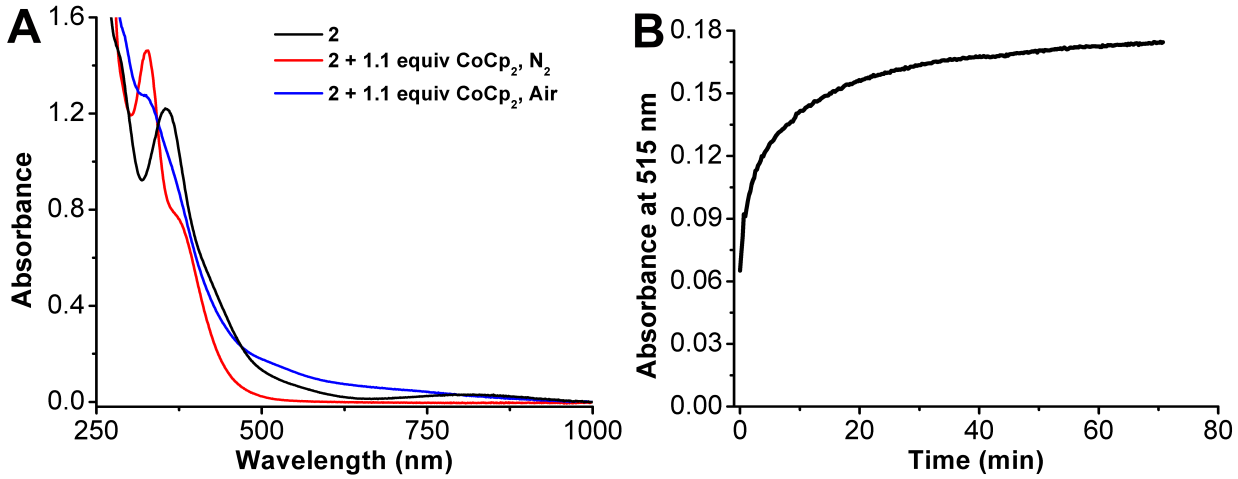

Figure S70. (A) UV-vis spectra of 80 μM solution of Mn(^{nPr}dhbpy)Cl **2** in MeCN (black) under N_2 with 1.1 equiv of $CoCp_2$ (red) and after being exposed to air for 70 min (blue). (B) Time versus absorbance at 515 nm upon exposure of an 80 μM solution of Mn(^{nPr}dhbpy)Cl with 1.1 equiv $CoCp_2$ to air. Conditions: quartz cuvette with 1 cm pathlength.

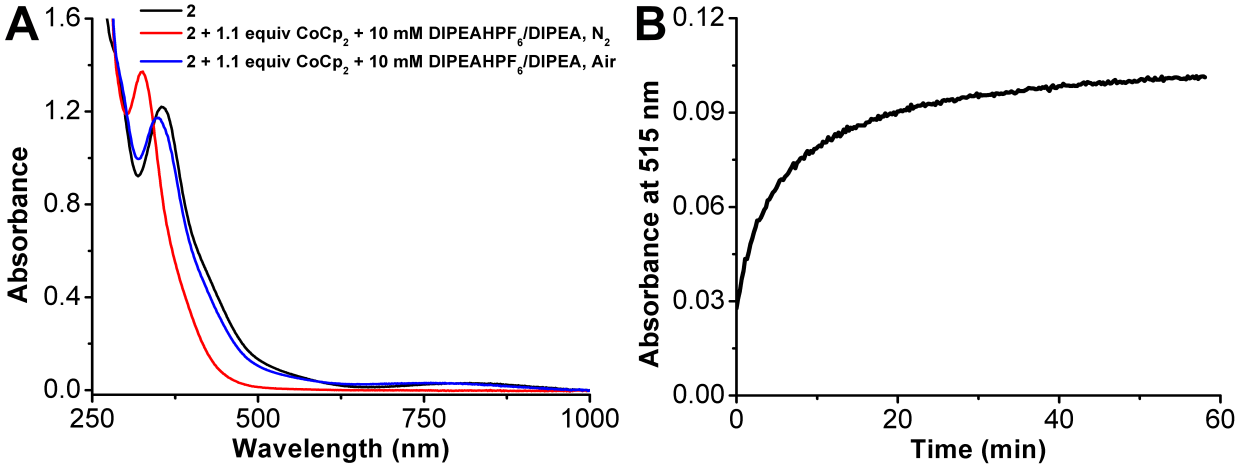

Figure S71. (A) UV-vis spectra of 80 μM solution of Mn(^{nPr}dhbpy)Cl **2** in MeCN (black) under N_2 with 1.1 equiv of $CoCp_2$ and 10 mM DIPEAHPF$_6$/DIPEA (red) and after being exposed to air for 60 min (blue). (B) Time versus absorbance at 515 nm upon exposure of an 80 μM solution of Mn(^{nPr}dhbpy)Cl with 1.1 equiv $CoCp_2$ and 10 mM DIPEAHPF$_6$/DIPEA to air. Conditions: quartz cuvette with 1 cm pathlength.

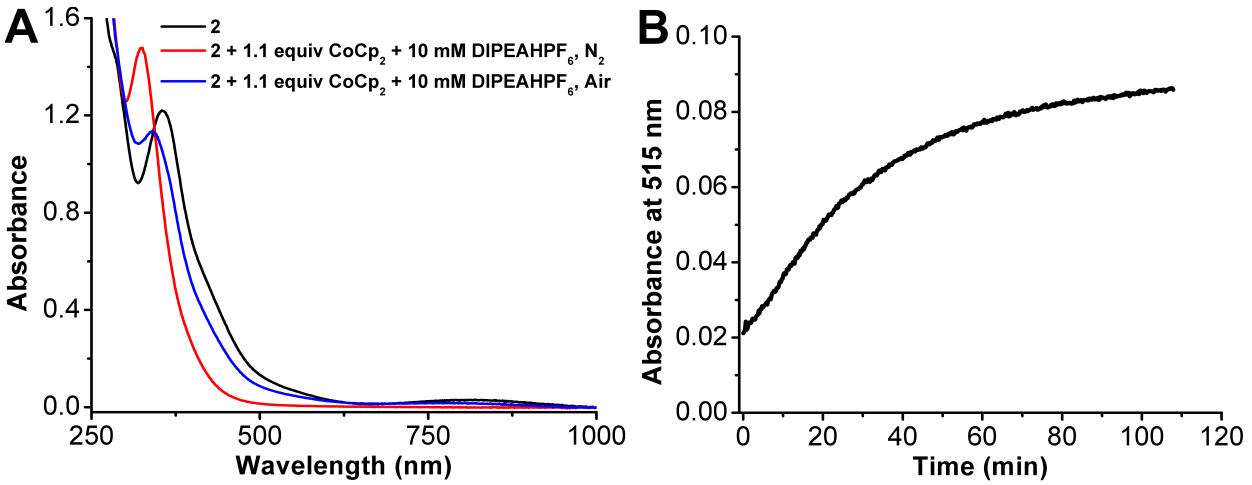

Figure S72. (A) UV-vis spectra of 80 μM solution of Mn(^{nPr}dhbpy)Cl **2** in MeCN (black) under N_2 with 1.1 equiv of $CoCp_2$ and 10 mM $DIPEAHPF_6$ (red) and after being exposed to air for 110 min (blue). (B) Time versus absorbance at 515 nm upon exposure of an 80 μM solution of Mn(^{nPr}dhbpy)Cl with 1.1 equiv $CoCp_2$ and 10 mM $DIPEAHPF_6$ to air. Conditions: quartz cuvette with 1 cm pathlength.

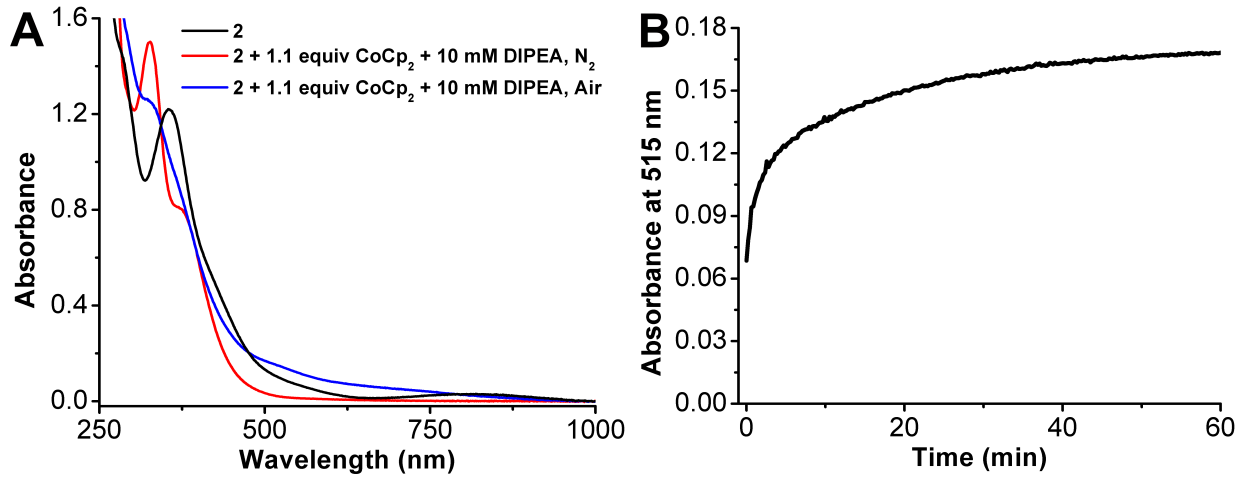

Figure S73. (A) UV-vis spectra of 80 μM solution of Mn(^{nPr}dhbpy)Cl **2** in MeCN (black) under N_2 with 1.1 equiv of $CoCp_2$ and 10 mM DIPEA (red) and after being exposed to air for 60 min (blue). (B) Time versus absorbance at 515 nm upon exposure of an 80 μM solution of Mn(^{nPr}dhbpy)Cl with 1.1 equiv $CoCp_2$ and 10 mM DIPEA to air. Conditions: quartz cuvette with 1 cm pathlength.

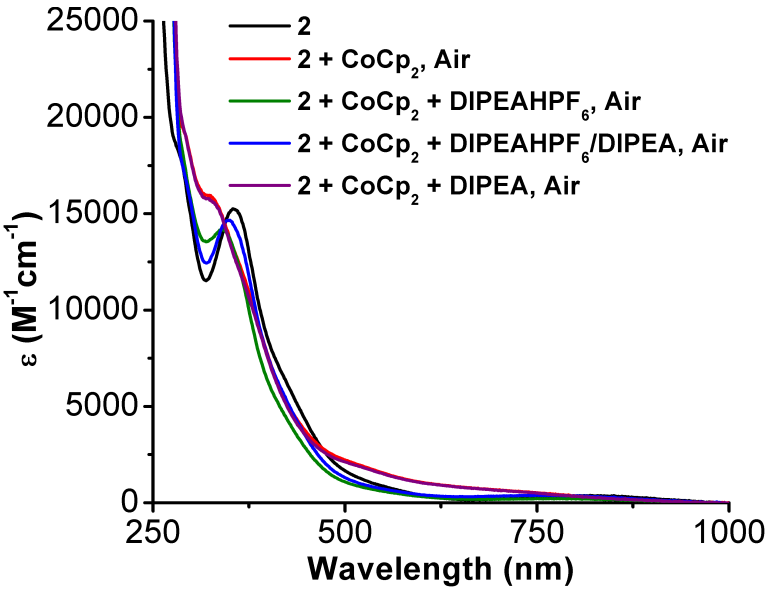

Figure S74. Overlay of data involving Mn(^{nPr}dhbpy)Cl **2** from **Figs S70-S73** after samples were allowed to react with air completely.

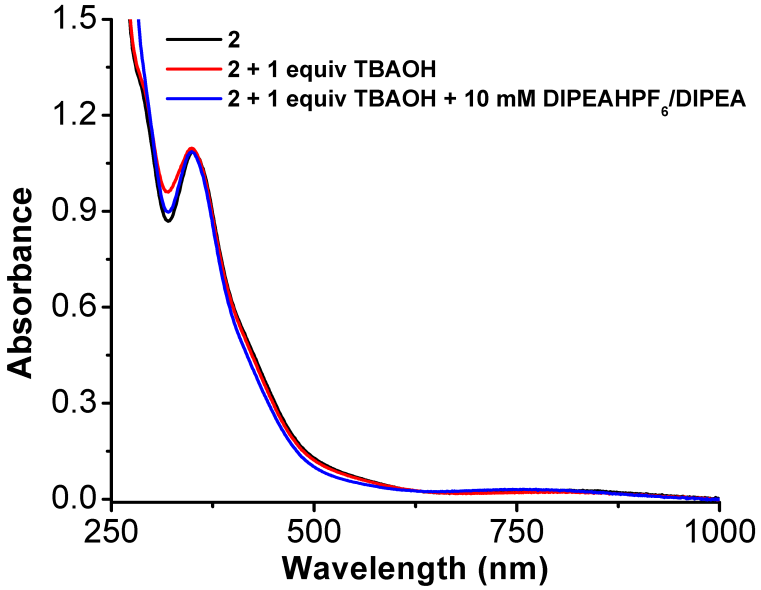

Figure S75. UV-vis spectra of 80 μM Mn(^{nPr}dhbpy)Cl **2** with (red) and without (black) 1 equiv TBAOH•30H_2O and with of 10 mM buffer (1:1 DIPEAHPF_6:DIPEA) in the presence of 1 equiv TBAOH•30H_2O (blue). Conditions: quartz cuvette with 1 cm pathlength.

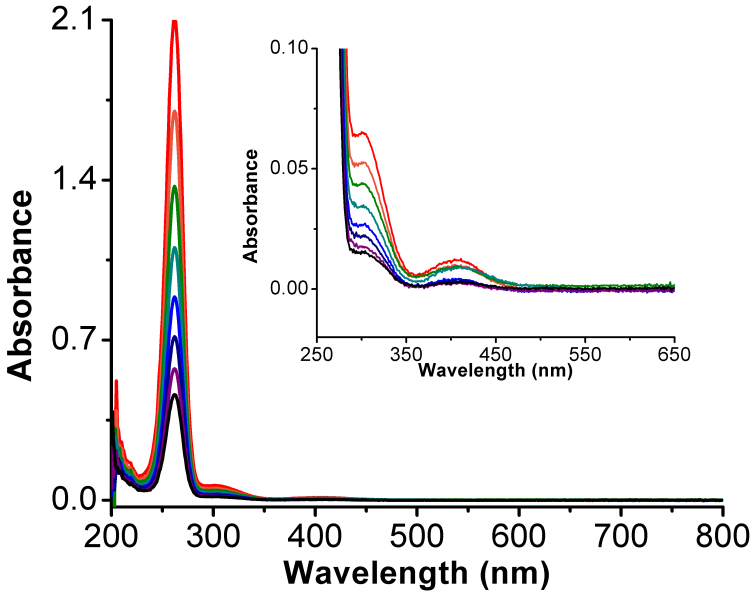

Figure S76. (A) UV-vis titration of $[CoCp_2][PF_6]$ in MeCN. Conditions: $[CoCp_2][PF_6]$ = 1.97 x 10^{-4}, 1.64 x 10^{-4}, 1.37 x 10^{-4}, 1.14 x 10^{-4}, 9.50 x 10^{-5}, 7.91 x 10^{-5}, 6.59 x 10^{-5}, 5.50 x 10^{-5} M; 1 cm pathlength cuvette.

Computational Methods

Geometry optimizations were performed without geometry constraints at the DFT level with the Gaussian 16 program, Rev B.01,[8] employing the hybrid functional B3LYP[9] and the def2-SVP basis set was used for all atoms.[10] Dispersion and bulk solvent effects (acetonitrile = MeCN) were accounted for at the optimization stage, by using Grimme's D3 parameter set with Becke-Johnson (BJ) damping[11] and the SMD continuum model,[12] respectively. The stationary points and their nature as minima (no imaginary frequencies) were characterized by vibrational analysis using the IGRRHO approach as implemented by default in the software package, which also produced enthalpy (H), entropy (S) and Gibbs energy (G) data at 298.15 K. The minima connected by a given transition state were determined by perturbing the transition states along the TS coordinate and optimizing to the nearest minimum. Free energies were corrected (ΔG_{qh}) to account for concentration effects and for errors associated with the harmonic oscillator approximation. Thus, according to Truhlars's quasi-harmonic approximation for vibrational entropy and enthalpy, all vibrational frequencies below 100 cm^{-1} were set to this value.[13] These anharmonic and concentration corrections were calculated with the Goodvibes code.[14] Concentrations were set at 0.001 M for metal complexes, 0.05 M for DIPEAH and DIPEA, 0.004 M for O_2 and 18.9 M for MeCN. Energies were refined by means of single point calculations with the ORCA 5.0 program,[15] employing the range-separated hybrid functional ωB97M-V[16] and the def2-TZVPP basis set.[17] Dispersion effects were treated with Grimme's D4 parameter set[18] according to the method of Najibi and Goerigk[19] and solvation again by the SMD model. The stability of the wavefunction and spin contamination were studied at the double- and triple-zeta levels of theory.

The labelling scheme for minima is $^{\text{multiplicity}}_{\text{charge}}\mathbf{Mn}(\boldsymbol{axial\ ligands})$ for metal complexes; the dianionic tetradentate ligand framework is a common feature of all Mn species and does not change its coordination mode during the reaction, so it is omitted in the notation where possible for clarity.

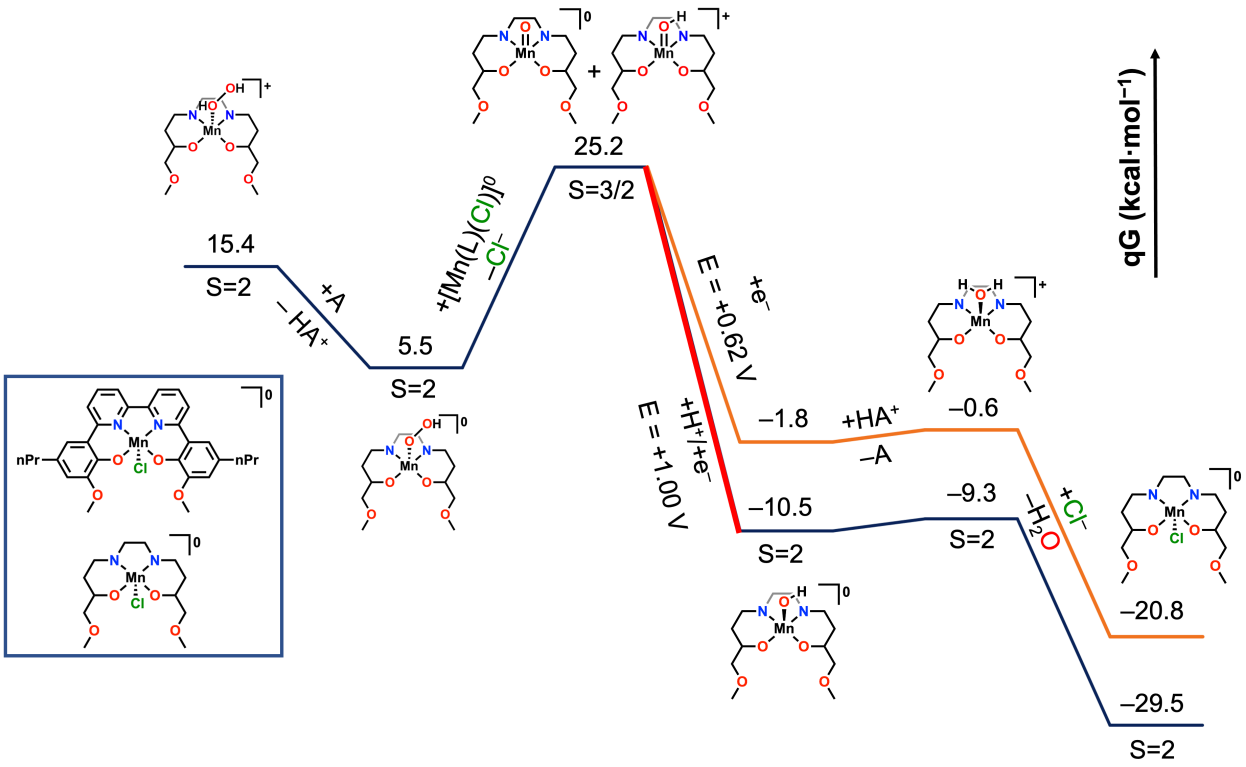

Figure S77. Free energy diagram of ORR by Mn(^{nPr}dhbpy)Cl **2** to H_2O.

Single Crystal Diffraction Studies

A single crystal of **2** Mn(^{nPr}dhbpy)Cl or DIPEAPF$_6$ was coated with Paratone oil and mounted on a MiTeGen MicroLoop. The X-ray intensity data were measured on a Bruker D8 Venture Photon III Kappa four-circle diffractometer system equipped with Incoatec IμS 3.0 micro-focus sealed X-ray tubes (Cu Kα, λ = 1.54178 Å; Mo Kα, λ = 0.71073 Å) and HELIOS double bounce multilayer mirror monochromators. The frames were integrated with the Bruker SAINT software package package[20] a narrow-frame algorithm. Data were corrected for absorption effects using the Multi-Scan method (SADABS).[21] Each structure was solved and refined using the Bruker SHELXTL Software Package[22] within APEX4[20] and OLEX2.[23] Non-hydrogen atoms were refined anisotropically. The N-H hydrogen atom in DIPEAHPF$_6$ was located in the electron density map and refined isotropically. All other hydrogen atoms in both structures were placed in geometrically calculated positions with U_{iso} = 1.2U_{equiv} of the parent atom (1.5U_{equiv} for methyl). The relative occupancy of the disordered atoms in each structure was freely refined, with constraints and restraints used on the anisotropic displacement parameters and bond lengths of the disordered F atoms only.

Table S14. Crystallographic details for Mn(^{nPr}dhbpy)Cl **2** and DIPEAHPF$_6$

	2 Mn(^{nPr}dhbpy)Cl	DIPEAHPF$_6$
CCDC number	2255849	2255850
Formula	$C_{64}H_{66}Cl_2Mn_2N_6O_8$	$C_8H_{20}F_6NP$
FW (g/mol)	1228.00	275.22
Temp (K)	100(2)	100(2)
λ (Å)	1.54178	0.71073
Size (mm)	0.030 x 0.047 x 0.505	0.085 x 0.088 x 0.122
Crystal habit	brown-yellow rod	colourless needle
Crystal system	monoclinic	monoclinic
Space group	P 2_1/c	P 2_1/n
a (Å)	15.3780(4)	8.2349(2)
b(Å)	9.8097(2)	17.2894(6)
c (Å)	20.2954(5)	8.9716(3)
α (°)	90	90
β (°)	109.0756(18)	97.3780(10)
γ (°)	90	90
Volume (Å^3)	2893.51(12)	1266.77(7)
Z	2	4
Density (g/cm^3)	1.409	1.443
μ (mm^{-1})	4.904	0.266
F(000)	1280	576
θ range (°)	3.04 to 68.36	2.36 to 28.29
Index ranges	-18 ≤ h ≤ 18 -11 ≤ k ≤ 10 -24 ≤ l ≤ 24	-10 ≤ h ≤ 10 -23 ≤ k ≤ 22 -10 ≤ l ≤ 11
Reflns collected	34823	30006
Independent reflns	5293 [R_{int} = 0.0881]	3123 [R_{int} = 0.0428]
Data / restraints /parameters	5293 / 0 / 404	3123 / 28 / 173
GOF on F^2	1.027	1.059
R_1 (I>2σ(I))	0.0505	0.0401
wR_2 (all data)	0.1376	0.1041

References

(1) Li, Q.; Batchelor-McAuley, C.; Lawrence, N. S.; Hartshorne, R. S.; Compton, R. G. Anomalous solubility of oxygen in acetonitrile/water mixture containing tetra-n-butylammonium perchlorate supporting electrolyte; the solubility and diffusion coefficient of oxygen in anhydrous acetonitrile and aqueous mixtures. *Journal of Electroanalytical Chemistry* **2013**, *688*, 328-335. DOI: https://doi.org/10.1016/j.jelechem.2012.07.039.

(2) Nichols, A. W.; Cook, E. N.; Gan, Y. J.; Miedaner, P. R.; Dressel, J. M.; Dickie, D. A.; Shafaat, H. S.; Machan, C. W. Pendent Relay Enhances H2O2 Selectivity during Dioxygen Reduction Mediated by Bipyridine-Based Co–N2O2 Complexes. *Journal of the American Chemical Society* **2021**, *143* (33), 13065-13073. DOI: 10.1021/jacs.1c03381.

(3) Hooe, S. L.; Rheingold, A. L.; Machan, C. W. Electrocatalytic Reduction of Dioxygen to Hydrogen Peroxide by a Molecular Manganese Complex with a Bipyridine-Containing Schiff Base Ligand. *Journal of the American Chemical Society* **2018**, *140* (9), 3232-3241. DOI: 10.1021/jacs.7b09027.

(4) Saba, S.; Hernandez, R.; Choy, C. C.; Carta, K.; Bennett, Y.; Bondi, S.; Kolaj, S.; Bennett, C. A simple and efficient one-step protocol for the preparation of alkyl-substituted ammonium

tetrafluoroborate and hexafluorophosphate salts. *Journal of Fluorine Chemistry* **2013**, *153*, 168-171. DOI: https://doi.org/10.1016/j.jfluchem.2013.05.007.
(5) Shivapurkar, R.; Jeannerat, D. Determination of the relative pKa's of mixtures of organic acids using NMR titration experiments based on aliased 1H–13C HSQC spectra. *Analytical Methods* **2011**, *3* (6), 1316-1322, 10.1039/C0AY00771D. DOI: 10.1039/C0AY00771D.
(6) Espinoza, E. M.; Clark, J. A.; Soliman, J.; Derr, J. B.; Morales, M.; Vullev, V. I. Practical Aspects of Cyclic Voltammetry: How to Estimate Reduction Potentials When Irreversibility Prevails. *Journal of The Electrochemical Society* **2019**, *166* (5), H3175. DOI: 10.1149/2.0241905jes.
(7) Hooe, S. L.; Machan, C. W. Dioxygen Reduction to Hydrogen Peroxide by a Molecular Mn Complex: Mechanistic Divergence between Homogeneous and Heterogeneous Reductants. *Journal of the American Chemical Society* **2019**, *141* (10), 4379-4387. DOI: 10.1021/jacs.8b13373. Anson, C. W.; Stahl, S. S. Cooperative Electrocatalytic O2 Reduction Involving Co(salophen) with p-Hydroquinone as an Electron-Proton Transfer Mediator. *Journal of the American Chemical Society* **2017**, *139* (51), 18472-18475. DOI: 10.1021/jacs.7b11362.
(8) *Gaussian 16 Rev. B.01*; Wallingford, CT, 2016.
(9) Becke, A. D. Density-functional thermochemistry. III. The role of exact exchange. *J. Chem. Phys.* **1993**, *98* (7), 5648-5652. DOI: doi:http://dx.doi.org/10.1063/1.464913. Lee, C.; Yang, W.; Parr, R. G. Development of the Colle-Salvetti correlation-energy formula into a functional of the electron density. *Phys. Rev. B* **1988**, *37* (2), 785-789. Vosko, S. H.; Wilk, L.; Nusair, M. Accurate spin-dependent electron liquid correlation energies for local spin density calculations: a critical analysis. *Can. J. Phys.* **1980**, *58* (8), 1200-1211. DOI: 10.1139/p80-159 (acccessed 2016/05/20). Stephens, P. J.; Devlin, F. J.; Chabalowski, C. F.; Frisch, M. J. Ab Initio Calculation of Vibrational Absorption and Circular Dichroism Spectra Using Density Functional Force Fields. *J. Phys. Chem.* **1994**, *98* (45), 11623-11627. DOI: 10.1021/j100096a001.
(10) Weigend, F.; Ahlrichs, R. Balanced basis sets of split valence, triple zeta valence and quadruple zeta valence quality for H to Rn: Design and assessment of accuracy. *Phys. Chem. Chem. Phys.* **2005**, *7* (18), 3297-3305, 10.1039/B508541A. DOI: 10.1039/B508541A. Weigend, F. Accurate Coulomb-fitting basis sets for H to Rn. *Phys. Chem. Chem. Phys.* **2006**, *8* (9), 1057-1065, 10.1039/B515623H. DOI: 10.1039/B515623H.
(11) Grimme, S.; Antony, J.; Ehrlich, S.; Krieg, H. A consistent and accurate ab initio parametrization of density functional dispersion correction (DFT-D) for the 94 elements H-Pu. *J. Chem. Phys.* **2010**, *132* (15), 154104. DOI: doi:http://dx.doi.org/10.1063/1.3382344. Grimme, S.; Ehrlich, S.; Goerigk, L. Effect of the damping function in dispersion corrected density functional theory. *J. Comput. Chem.* **2011**, *32* (7), 1456-1465. DOI: 10.1002/jcc.21759.
(12) Marenich, A. V.; Cramer, C. J.; Truhlar, D. G. Universal solvation model based on solute electron density and on a continuum model of the solvent defined by the bulk dielectric constant and atomic surface tensions. *Journal of Physical Chemistry B* **2009**, *113* (18), 6378-6396. DOI: 10.1021/jp810292n.
(13) Ribeiro, R. F.; Marenich, A. V.; Cramer, C. J.; Truhlar, D. G. Use of Solution-Phase Vibrational Frequencies in Continuum Models for the Free Energy of Solvation. *J. Phys. Chem. B* **2011**, *115* (49), 14556-14562. DOI: 10.1021/jp205508z.
(14) *Goodvibes v3.0.1*; 2019. https://doi.org/10.5281/zenodo.3346166.
(15) Neese, F. Software update: The ORCA program system—Version 5.0. *WIREs Computational Molecular Science* **2022**, *n/a* (n/a), e1606, https://doi.org/10.1002/wcms.1606. DOI: https://doi.org/10.1002/wcms.1606.

(16) Mardirossian, N.; Head-Gordon, M. ωB97M-V: A combinatorially optimized, range-separated hybrid, meta-GGA density functional with VV10 nonlocal correlation. *The Journal of Chemical Physics* **2016**, *144* (21), 214110. DOI: 10.1063/1.4952647.
(17) Weigend, F.; Ahlrichs, R. Balanced basis sets of split valence, triple zeta valence and quadruple zeta valence quality for H to Rn: Design and assessment of accuracy. *Physical Chemistry Chemical Physics* **2005**, *7* (18), 3297-3305. DOI: 10.1039/b508541a. Weigend, F. Accurate Coulomb-fitting basis sets for H to Rn. *Physical Chemistry Chemical Physics* **2006**, *8* (9), 1057-1065. DOI: 10.1039/b515623h. Hellweg, A.; Hättig, C.; Höfener, S.; Klopper, W. Optimized accurate auxiliary basis sets for RI-MP2 and RI-CC2 calculations for the atoms Rb to Rn. *Theoretical Chemistry Accounts* **2007**, *117* (4), 587-597. DOI: 10.1007/s00214-007-0250-5.
(18) Caldeweyher, E.; Bannwarth, C.; Grimme, S. Extension of the D3 dispersion coefficient model. *The Journal of Chemical Physics* **2017**, *147* (3), 034112. DOI: 10.1063/1.4993215 (acccessed 5/15/2023). Caldeweyher, E.; Ehlert, S.; Hansen, A.; Neugebauer, H.; Spicher, S.; Bannwarth, C.; Grimme, S. A generally applicable atomic-charge dependent London dispersion correction. *The Journal of Chemical Physics* **2019**, *150* (15), 154122. DOI: 10.1063/1.5090222 (acccessed 5/15/2023).
(19) Najibi, A.; Goerigk, L. DFT-D4 counterparts of leading meta-generalized-gradient approximation and hybrid density functionals for energetics and geometries. *Journal of Computational Chemistry* **2020**, *41* (30), 2562-2572, https://doi.org/10.1002/jcc.26411. DOI: https://doi.org/10.1002/jcc.26411.
(20) *Saint; APEX4*; Bruker AXS Inc.: Madison, Wisconsin, USA, 2019.
(21) Krause, L.; Herbst-Irmer, R.; Sheldrick, G. M.; Stalke, D. Comparison of silver and molybdenum microfocus X-ray sources for single-crystal structure determination. *Journal of Applied Crystallography* **2015**, *48* (1), 3-10. DOI: 10.1107/S1600576714022985.
(22) Sheldrick, G. M. SHELXT - Integrated space-group and crystal-structure determination. *Acta Crystallographica* **2015**, *71* (1), 3-8. DOI: 10.1107/S2053273314026370.
(23) Dolomanov, O. V.; Bourhis, L. J.; Gildea, R. J.; Howard, J. A. K.; Puschmann, H. OLEX2: A Complete Structure Solution, Refinement and Analysis Program. *Journal of Applied Crystallography* **2009**, *42*, 339-341. DOI: 10.1107/S0021889808042726.